

PROCEEDINGS OF SPIE

[SPIDigitalLibrary.org/conference-proceedings-of-spie](https://spiedigitallibrary.org/conference-proceedings-of-spie)

On finding optimal speckle filtering for extraction of vegetation biophysical information using Sentinel-1 SAR imagery

Ali, Syamani D., Fithria, Abdi, Rahmadi, Adi, Rezekiah, Arfa Agustina

Syamani D. Ali, Abdi Fithria, Adi Rahmadi, Arfa Agustina Rezekiah, "On finding optimal speckle filtering for extraction of vegetation biophysical information using Sentinel-1 SAR imagery," Proc. SPIE 12082, Seventh Geoinformation Science Symposium 2021, 120820V (22 December 2021); doi: 10.1117/12.2615135

SPIE.

Event: Seventh Geoinformation Science Symposium (GSS 2021), 2021, Yogyakarta, Indonesia

On Finding Optimal Speckle Filtering for Extraction of Vegetation Biophysical Information Using Sentinel-1 SAR Imagery

Syamani D. Ali^{*a}, Abdi Fithria^a, Adi Rahmadi^a, Arfa Agustina Rezekiah^a

^aFaculty of Forestry, University of Lambung Mangkurat, Jl. Ahmad Yani km. 35, Banjarbaru, 70714, South Kalimantan, Indonesia

ABSTRACT

The SAR imagery such as Sentinel-1 in general has a major problem with the speckle effects. There are many speckle filtering methods have been developed to reduce the speckle effect. This research aims to test the ability of a number of speckle filtering methods to extract vegetation biophysical information from Sentinel-1. The ground truth of vegetation biophysical information in this research were simulated using Sentinel-2 MSI imagery. That is, Leaf Area Index (LAI), Canopy Water Content (CWC), Canopy Chlorophyll Content (CCC), Fraction of Vegetation Cover (FVC), and Fraction of Absorbed Photosynthetically Active Radiation (FAPAR). The Sentinel-1 imagery was speckle filtered using various methods, namely Lee, Lee Sigma, Refined Lee, IDAN, Boxcar, Frost, Gamma Map, and Median. Some speckle filtering parameters were modified, i.e., the processing windows. The Dual Polarization SAR Vegetation Index (DPSVI) were then extracted from the speckle-filtered Sentinel-1. DPSVI were then tested for correlation with vegetation biophysical information using the Pearson Correlation Coefficient (r). The test results show that Boxcar produces the highest r values for all types of vegetation biophysical information, with values ranging from 0.6s to 0.7s. Followed by Lee, Gamma Map, Median, and Frost. Each with a processing window size of 21x21. Since there are no r values was found which reached 0.8 for processing window sizes up to 21x21, the simulation was then run using the regression method. The simulation results show that to achieve r values of 0.8, it is predicted that window sizes range from 35x35 to 93x93.

Keywords: Speckle filtering, Synthetic Aperture Radar, Sentinel-1, Sentinel-2, vegetation biophysics, correlation

*syamani.fhut@ulm.ac.id; phone 62 511 478-0886; fax 62 511 478-0886; ulm.ac.id

1. INTRODUCTION

The ability of multispectral optical imageries such as Landsat series, Sentinel-2 MSI, Sentinel-3 OLCI, or others, in extracting vegetation biophysical information above the earth's surface is unquestionable. Various research results have proven this. Ref. 9 validated the Sentinel Simplified Level 2 Product Prototype Processor (SL2P) for mapping cropland biophysical variables using Sentinel-2 MSI and Landsat-8 OLI data. They found that SL2P presents good performances to estimate Leaf Area Index (LAI) and Fraction of Vegetation Cover (FVC) from both MSI and OLI data. Ref. 31 conducted a mapping and monitoring of woody vegetation canopy cover and height at a regional scale using Landsat time-series data, from 2000 to 2017. They found that tree height estimates had a correlation coefficient of 0.92 and the r^2 of 0.85. Ref. 16 estimates LAI for Landsat imageries over the contiguous United States. They found that LAI estimates show an overall Root Mean Squared Error (RMSE) of 0.8 with r^2 of 0.88. Ref. 44 used the Sentinel-3 Ocean and Land Color Instrument (OLCI) to derive LAI information. Field measurements of LAI at two forest sites quantitatively confirm that the estimated LAI from OLCI is reasonably accurate with $r^2 > 0.65$ and $RMSE < 1.00 \text{ m}^2\text{m}^{-2}$ 44. Ref. 8 validated the extracted LAI information using Sentinel-2 Level 2 Prototype Processor (SL2P) and modified version of Sentinel-2 Level 2 Prototype Processor (SL2P-D). The results showed that both of them demonstrated good performance, with SL2P-D slightly more accurate than SL2P.

In fact, there are countless research that prove the power of optical imageries in extracting vegetation biophysical information. However, optical imageries such as Sentinel-2 MSI have a major drawback, which is that they are very sensitive to atmospheric disturbances. For tropical areas such as Indonesia, which always experience the presence of atmospheric disturbances such as clouds, monitoring the vegetation biophysical information throughout time continuously is a special challenge. Ref. 13 stated that a dense time series of optical satellite imagery describing vegetation activity provides essential information for the efficient and regular monitoring of vegetation. Nevertheless, the temporal resolution of optical sensors is strongly affected by cloud cover, resulting in significant missing information¹³. The use of

complementary acquisitions, such as Synthetic Aperture Radar (SAR) data, opens the door to the development of new multi-sensor methodologies aiming at the reconstruction of missing information¹³.

Recently, there are many SAR imaging technologies that have been developed, which can be used to extract vegetation biophysical information. Such as the Advanced Land Observing Satellite-Phased Array L-band Synthetic Aperture Radar (ALOS-PALSAR), the Envisat Advanced Synthetic Aperture Radar (ASAR), and the successor to Envisat ASAR, the Sentinel-1 SAR, which is operated by the European Space Agency (ESA). Since its presence in 2014, Sentinel-1 has attracted the attention of practitioners and researchers of radar remote sensing. Given that Sentinel-1 has a fairly high spatial and temporal resolution, it is also freely available to the public. In addition, Sentinel-1 released to the public has dual polarization, namely VV and VH. With high spatial and temporal resolution, as well as the availability of free and real time data, this makes Sentinel-1 SAR very feasible to be used in monitoring vegetation biophysical information.

Various research have been carried out to extract vegetation biophysical information from the Sentinel-1 SAR imagery. Ref. 30 developed the Dual Polarization SAR Vegetation Index (DPSVI) for biomass information retrieval using Sentinel-1. The results showed that between DPSVI and Above Ground Biomass (AGB) had r^2 values of 0.7 and above. Ref. 24 derives a new vegetation index from dual-pol SAR, namely the Dual-polarimetric Radar Vegetation Index (DpRVI). Their research results show that DpRVI has r^2 values ranging from 0.7s to 0.8s for certain vegetation biophysical parameters. There is one model that is often used as a method for extracting vegetation biophysical information from SAR imageries such as Sentinel-1, namely the Water Cloud Model (WCM)^{2,15}. There has been a considerable amount of research using WCM to extract vegetation biophysical information from Sentinel-1. For examples Ref. 3, 4, 5, 25, 43, and so on.

Despite the fact that SAR imagery such as Sentinel-1 has advantages over optical imageries in terms of minimizing atmospheric effects, it has one major drawback, namely the presence of speckle effects. Speckles are a direct result of the coherent incident energy, which can be assumed to have a single frequency and the wavefront arrives at a single-phase pixel³³. Speckle, appearing in Synthetic Aperture Radar (SAR) imageries as granular noise, is due to the interference of waves reflected from many elementary scatterers²². The speckle appears in SAR imageries due to the phenomenon of backscattering complexity of objects on the earth's surface³⁸. Speckle in SAR imageries complicates the imagery interpretation problem by reducing the effectiveness of image segmentation and classification²². This is a distinct advantage for multispectral optical images such as Sentinel-2, because it does not have the presence of a speckle effect. Even though the optical imageries have problems with atmospheric particles.

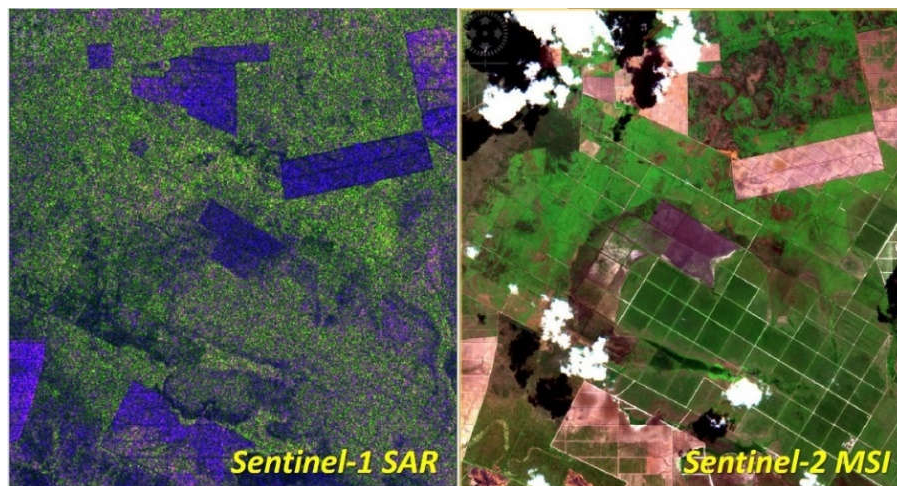


Fig. 1. Sentinel-1 and Sentinel-2 at the same location and acquisition date. SAR imagery is relatively clean from atmospheric disturbances, but is decorated by speckle effects. Optical imagery has no speckle effect but is susceptible to atmospheric disturbances.

Heretofore, there are many speckle filtering methods that have been developed to reduce the speckle effect on radar imageries. Such as Lee¹⁹, Lee Sigma^{20,21}, Refined Lee⁴⁵, Boxcar²³, Frost¹², Gamma Map⁶, and Intensity-Driven Adaptive-Neighborhood (IDAN)⁴⁰. Each speckle filtering method has different effects and capabilities. Even the same speckle filtering method can also be modified some parameters, for example the window processing size. There are quite a number of previous studies that have tested the capabilities of each speckle filtering technique. As has been implemented by Ref. 1, 7, 10, 11, 14, 18, 26, 28, 32, 35, and 39.

Ref. 14 tested the performance of various speckle filtering methods on Sentinel-1, namely Frost, Gamma-MAP, Median, and Refined Lee, for modeling forest aboveground biomass (AGB). Their research results show that Frost provides the best correlation between AGB and backscatter. The value of r^2 is 0.3464158 and RMSE is 33.5231. Ref. 26 evaluated a number of speckle filtering methods for Polarimetric SAR (PolSAR) data. The filter methods tested were Boxcar, Lee Sigma, Refined Lee, Lopez, and IDAN. They found that IDAN was the best, because it had the smallest bias among all evaluated filter methods. However, they also found that the Boxcar was visually effective in reducing speckle. Although in the Boxcar filter results a lot of detail is lost due to blurring. Ref. 28 assessed a number of speckle filtering methods for the purposes of Object Based Image Analysis (OBIA). They found that the NL-SAR filter gave the best results. Ref. 30 uses the Refined Lee method to reduce noise on Sentinel-1, when testing the correlation between DPSVI and AGB. The results showed that the value of r^2 was in the range of 0.7s. Although in the research, Ref. 30 did not provide any argument for using Refined Lee.

Taking into account the advantages provided by SAR imageries such as Sentinel-1 in providing continuity of vegetation biophysical information, while SAR imageries themselves have problems with speckle effects. Of course, it is very necessary to test the ability of each speckle filtering method in reducing the speckle effect on SAR imageries. Especially when the SAR image will be used to extract vegetation biophysical information. The aim of this research is to test the ability of a number of speckle filtering methods to extract vegetation biophysical information from Sentinel-1 SAR. The expected significance of the results of this research is to obtain practical information about the most optimal speckle filtering techniques and parameters, in order to extract vegetation biophysical information from Sentinel-1 SAR imagery.

2. RESEARCH LOCATION AND DATA

2.1 Research Location

This research took samples of Sentinel-1 and Sentinel-2 in the southern part of Kalimantan or Borneo Island, Indonesia. This area covers the entire 50MKB Sentinel-2 MSI imagery tile area, with an area approximate to 110 kilometers x 110 kilometers. Administratively, most of this research area belongs to South Kalimantan Province, and a small part belongs to Central Kalimantan Province.

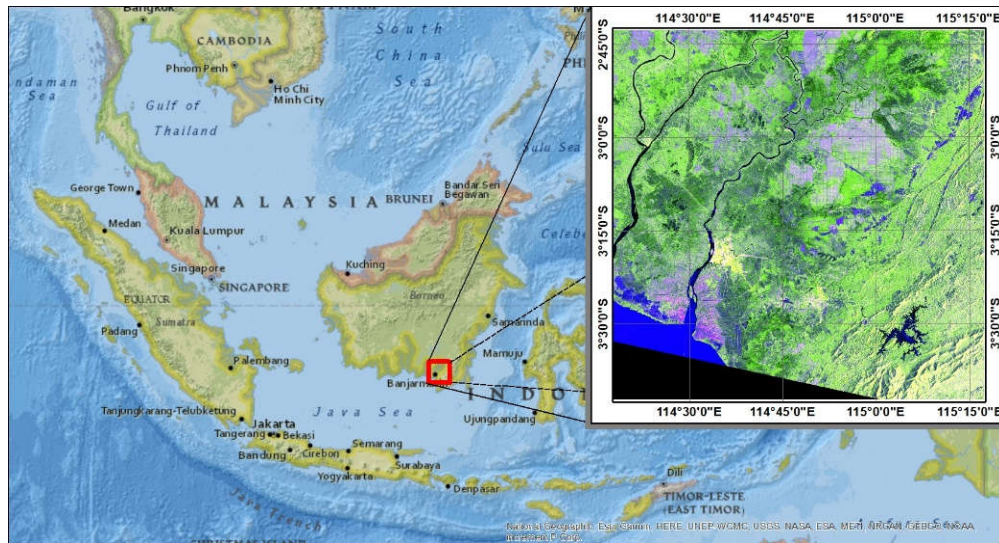


Fig. 2. The research location is in the southern part of Kalimantan Island, Indonesia

The main reason for choosing this research area is because the vegetation cover conditions in this area are very heterogeneous. Which consists of primary dryland forest, secondary dryland forest, swamp forest, peatland forest, mangrove forest, plantation forest, rubber plantation, oil palm plantation, mixed garden, fields/moorlands, rice fields, shrubs and bushes, swamp shrubs and bushes, and grasslands. The heterogeneity of vegetation features is very important in sampling for accuracy testing in this research. So that later the resulting accuracy can represent or at least approach the overall condition of the vegetation features.

2.2 Satellite Imageries

There are two satellite imageries used in this, namely Sentinel-1 Synthetic Aperture Radar (SAR) and Sentinel-2 Multispectral Instrument (MSI). Where both imageries are provided by the European Space Agency (ESA) free of charge. The selection process of the two imageries was done in such a way that the acquisition date of the two imageries is exactly the same. This is to ensure that there are no differences or changes in vegetation conditions in the two imageries. The Sentinel-1 SAR Interferometric Wide (IW) swath Ground Range Detected (GRD) product imagery used is S1A_IW_GRDH_1SDV_20190730T215953_20190730T220018_028352_03342D_4B6F, acquired on 30 July 2019, 21:59:53 GMT or 05:59:53 local time (Central Indonesia Time). The Sentinel-2 MSI imagery used is S2B_MSIL2A_20190730T022559_N0213_R046_T50MKB_20190730T062914, acquired on 30 July 2019, at 02:25:59 GMT or 10:25:59 local time. The Sentinel-2 (tile 50MKB) imagery used is Sentinel-2B level 2A Bottom of Atmospheric (BOA) reflectance and has been topographically corrected by ESA, considering that later vegetation biophysical information would be extracted quantitatively from Sentinel-2.

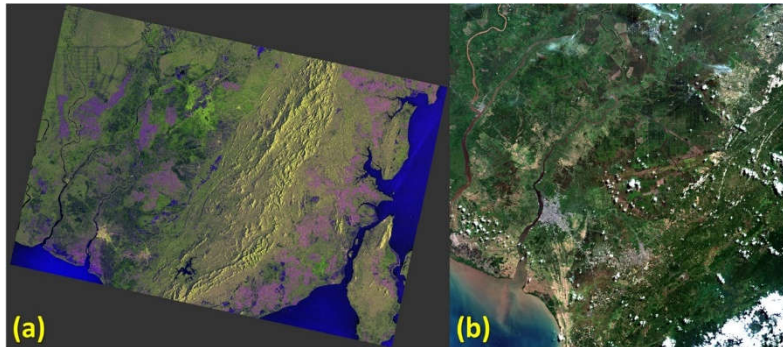


Fig. 3. (a) Sentinel-1 SAR IW swath GRD and (b) Sentinel-2 MSI level 2A tile 50MKB were used in this research.

2.3 Vegetation Biophysical Information

There are no ground surveys were conducted in this research. The ground truth of vegetation biophysical information in this research was simulated using vegetation biophysical information extracted quantitatively from MSI Sentinel-2 imagery. In this case, vegetation biophysical information was extracted automatically using the S2 SNAP Toolbox biophysical variable⁴², which is integrated in the Sentinel Application Platform (SNAP) software provided free of charge by the ESA. There are five vegetation biophysical information that would be extracted using this tool, namely Leaf Area Index (LAI), Canopy Water Content (CWC), Canopy Chlorophyll Content (CCC), Fraction of Vegetation Cover (FVC), and Fraction of Absorbed Photosynthetically Active Radiation (FAPAR).

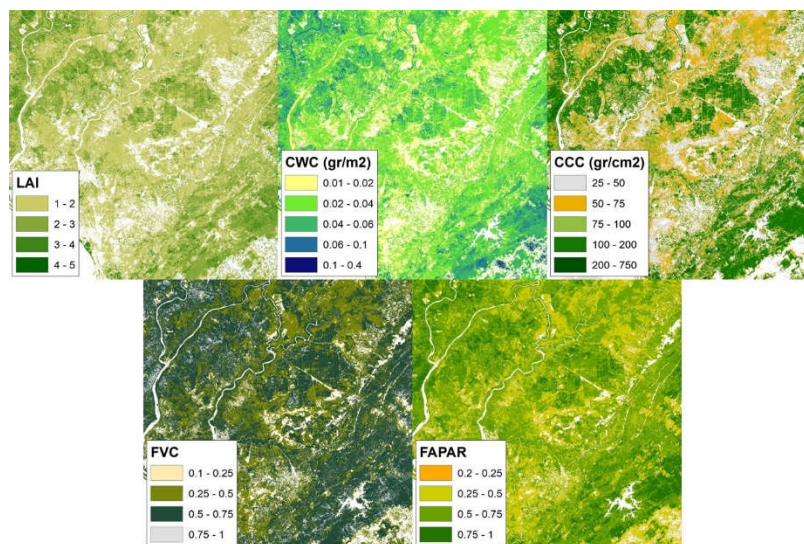


Fig. 4. Vegetation biophysical information extracted from Sentinel-2 MSI imagery.

It is certain that vegetation biophysical information from Sentinel-2 will not be as accurate as information directly from the field. However, this research will at least get an overview of the relative capabilities especially when compared to each other for each speckle filtering method in extracting vegetation biophysical information. When tested in the African semi-arid agricultural landscape, LAI products extracted from Sentinel-2 using SNAP application, were found to have r^2 of 0.6 to 0.7 with in-situ data. With a fairly large Mean Absolute Error (MAE), which is $> 2 \text{ m}^2\text{m}^{-2}$ ¹⁷.

3. RESEARCH METHODOLOGY

3.1 Image Pre-Processing

The dual-polarized (VV, VH) Sentinel-1 SAR imagery calibrated into normalized Radar Cross Section (RCS), Sigma Nought (σ^0), using Sentinel-1 Toolbox (S1TBX) in SNAP application. The imagery is then multilooked and co-registered using SRTM 1-arc second, so that the spatial resolution becomes 10 meters. The level 2A pre-orthorectified Sentinel-2 MSI imagery is resampled using Sentinel-2 Toolbox (S2TBX) in SNAP application, so that all bands have a spatial resolution of 10 meters. Furthermore, for analysis purposes, the Sentinel-1 swath is then crop to adjust it to the Sentinel-2 tile 50MKB area boundary.

3.2 Speckle Filters

Speckle filters are implemented on the calibrated and cropped Sentinel-1 imagery. There are several speckle filters to test, all of which are already available in the SNAP application tools. The speckle filters tested were Lee, Lee Sigma, Refined Lee, Frost, Gamma Map, Median, and IDAN. Several parameters in each speckle filtering method were modified, i.e., processing window sizes. The processing window sizes are set to vary, from 3x3 to 21x21. This applies to all speckle filtering methods, except Refined Lee and IDAN, which keep the default settings. Specifically for Lee Sigma, there are two variable parameter settings, namely processing window sizes and target window sizes. For Lee Sigma, the processing window sizes are set from 5x5 to 17x17, because the setting modes available in the SNAP application are indeed limited to those sizes. Meanwhile, for Lee Sigma's target window sizes, there are only two setting options, namely 3x3 and 5x5.

3.3 Dual Polarization SAR Vegetation Index (DPSVI)

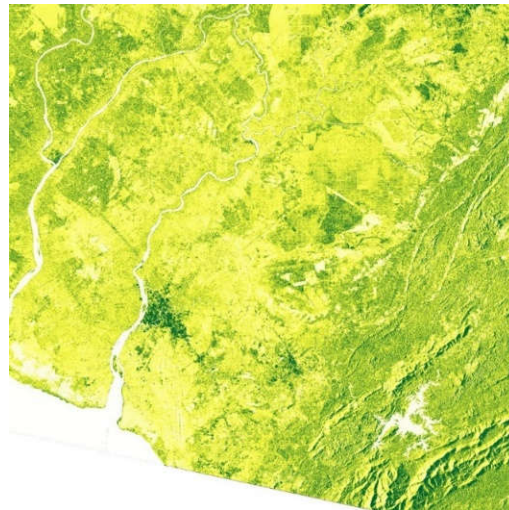


Fig. 5. DPSVI image using IDAN speckle filtering.

The Dual Polarization SAR Vegetation Index (DPSVI) was developed to extract vegetation biomass information³⁰. The DPSVI is designed for dual-polarized SAR imageries. DPSVI is implemented on each Sentinel-1 imagery which has been speckle filtered. DPSVI is formulated as follows³⁰:

$$DPSVI = \frac{\sigma_{vh(i)}^0 \left[\left(\sigma_{vv(max)}^0 \sigma_{vh(i)}^0 - \sigma_{vv(i)}^0 \sigma_{vh(i)}^0 + \sigma_{vh(i)}^0 \right) + \left(\sigma_{vv(max)}^0 \sigma_{vv(i)}^0 - \sigma_{vv(i)}^0 + \sigma_{vh(i)}^0 \sigma_{vv(i)}^0 \right) \right]}{\sqrt{2} * \sigma_{vv(i)}^0} \quad (1)$$

Where:

σ_{VH}^0 : Sigma nought calibrated Sentinel-1 Vertical-Horizontal (VH) polarization

σ_{VV}^0 : Sigma nought calibrated Sentinel-1 Vertical-Vertical (VV) polarization

$\sigma_{\text{VV(max)}}^0$: Maximum value of sigma nought calibrated Sentinel-1 Vertical-Vertical (VV) polarization

Just like the Normalized Difference Vegetation Index (NDVI) [34], DPSVI is proportional to vegetation biophysical information. For example, the higher the DPSVI value, the higher the vegetation biomass would be. Referring to Ref. 30 research, DPSVI is accurate enough to extract vegetation biophysical information from dual-polarized C-band SAR imageries such as Sentinel-1. Therefore, in this research, DPSVI is used as a parameter to test the ability of each speckle filtering method on Sentinel-1 imagery to extract vegetation biophysical information.

3.4 Accuracy Assessment and Sampling

The accuracy assessment is carried out using the Pearson Correlation Coefficient (PCC) (r), which is formulated as follows⁴¹:

$$r = \frac{\sum_{i=1}^n (x_i - \bar{x})(y_i - \bar{y})}{\sqrt{\sum_{i=1}^n (x_i - \bar{x})^2} \sqrt{\sum_{i=1}^n (y_i - \bar{y})^2}} \quad (2)$$

Where:

x_i : the i^{th} pixel of Sentinel-1 DPSVI

y_i : the i^{th} pixel of Sentinel-2 vegetation biophysical information

n : number of sample pixels

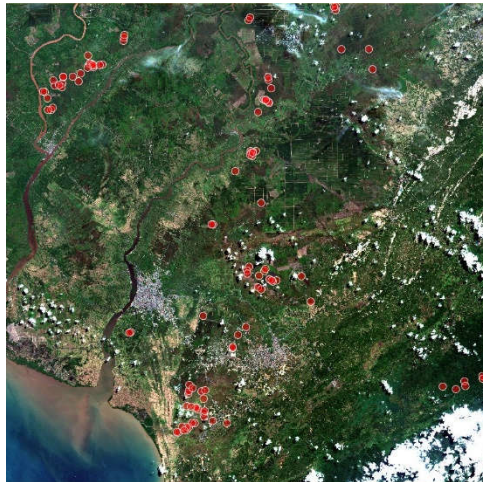


Fig. 6. Distribution of sample locations on Sentinel-2 MSI true color composite imagery.

In the calculation of PCC (r), a sample of a number of pixels is required. The distribution and designation of sample pixels is carried out with the help of the NDVI transformation of Sentinel-2 imagery. This is because NDVI has been shown to have a fairly strong correlation with vegetation biophysical information. The distribution of sample pixels was carried out by stratified purposive sampling. First, the vegetation features are separated from the non-vegetative features in NDVI. The technique is to use Otsu Thresholding²⁹. In this research, the Otsu Thresholding process was carried out using the free software Fiji is just ImageJ (Fiji)^{36,37}. From the results of Otsu Thresholding, a threshold value of 0.3 is obtained, this means that the NDVI value of 0.3 to 1 is confirmed to be vegetation features. The NDVI values of 0.3 to 1 are then stratified into ten strata. Next, the sample pixels are distributed purposively in each stratum. The distribution of these sample pixels is sufficient to represent almost all types of land cover in the study area, such as dryland forest, swamp forest, peatland forest, mangrove forest, plantation forest, rubber plantation, oil palm plantation, mixed garden, fields/moorlands, rice fields, shrubs and bushes, swamp shrubs and bushes, and grasslands. In sampling, there are several areas to avoid, i.e., areas covered by clouds or cloud shadows on Sentinel-2 imagery, and areas experiencing geometric distortion on Sentinel-1 imagery, i.e., shadow, foreshortening, or layover.

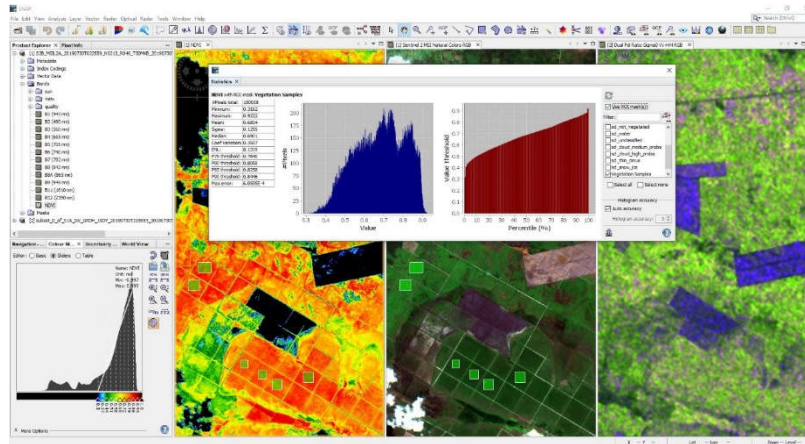


Fig. 7. Determination of sample pixels was done by stratified purposive sampling.

There are a total of more than 100,000 pixels set as samples. In the designation of sample pixels, the statistical distribution of NDVI values is of great concern. In this case, the distribution of pixel values of the NDVI sample is attempted to approach the normal distribution, although it cannot be completely normal, as shown in Fig. 6. Using the sample pixels, the PCC is then calculated in pairs between the DPSVI results from a certain speckle filtering method, and one of the variables from the vegetation biophysical information from Sentinel-2. For example, PCC between DPSVI filtered by Lee's method with a processing window size of 3x3 with LAI. And so on for other speckle filtering methods and other vegetation biophysical information variables.

3.5 Window Size Simulation

The target to be achieved in the search for the most optimal speckle filtering methods is to find a PCC value that reaches 0.8. Or in other words, the results of speckle filtering with vegetation biophysical information have a very strong correlation. If there is no PCC value that reaches 0.8 up to a processing window size of 21x21, then a simulation would be carried out to find the most optimal processing window size, so that later a PCC value of 0.8 can be obtained. The simulation of the processing window size was carried out using the regression method, based on the data of known PCC values up to the processing window size of 21x21. In this case, a scoring method is used on the processing window sizes. Namely, size 3x3 would be given a score of 3, size 5x5 would be given a score of 5, and so on, until size 21x21 would be given a score of 21. In the construction process of processing window size regression models, PCC values would be assigned as independent variables (x-axis). Meanwhile the processing window sizes would be placed as the dependent variable (y axis). The regression models applied are linear, exponential, logarithmic, power, and polynomial (quadratic). The regression equation which later has the highest correlation coefficient (r^2) is considered the best model to predict the most optimal processing window size in speckle filtering.

4. RESULT AND DISCUSSIONS

The many speckle filtering methods that are already available sometimes cause confusion when extracting certain information from SAR images such as Sentinel-1. This is the main thing that underlies this research. Indeed, up to now, there have been many studies comparing various speckle filtering methods. Either speckle filtering for things that are general, or specific for extracting vegetation information as is done in this research. From the point of view of SAR imagery, vegetation has its own characteristics based on its backscattering of electromagnetic waves burst by the SAR sensor. SAR technology is able to capture or distinguish between surface or specular features such as water and bare lands, double bounce features such as tall buildings or towers, and volumetric features such as vegetation canopy²⁷.

In this case, vegetation can have only volume scattering characteristics or a combination of volume scattering and double reflection scattering. If the vegetation has standing stems like trees, it will have a double bounce and scattering volume simultaneously. However, if the vegetation has only the structure of leaves and twigs without a stem, like a bush, then it will only have a scattering volume. Since speckle originating from the coherent summation of many individual feature scattering events within a pixel²⁷, vegetation features are among those that are quite problematic with speckle effects. This is caused by the structure of branches, twigs, and leaves of vegetation which will scatter electromagnetic waves from the SAR sensor in various directions irregularly.

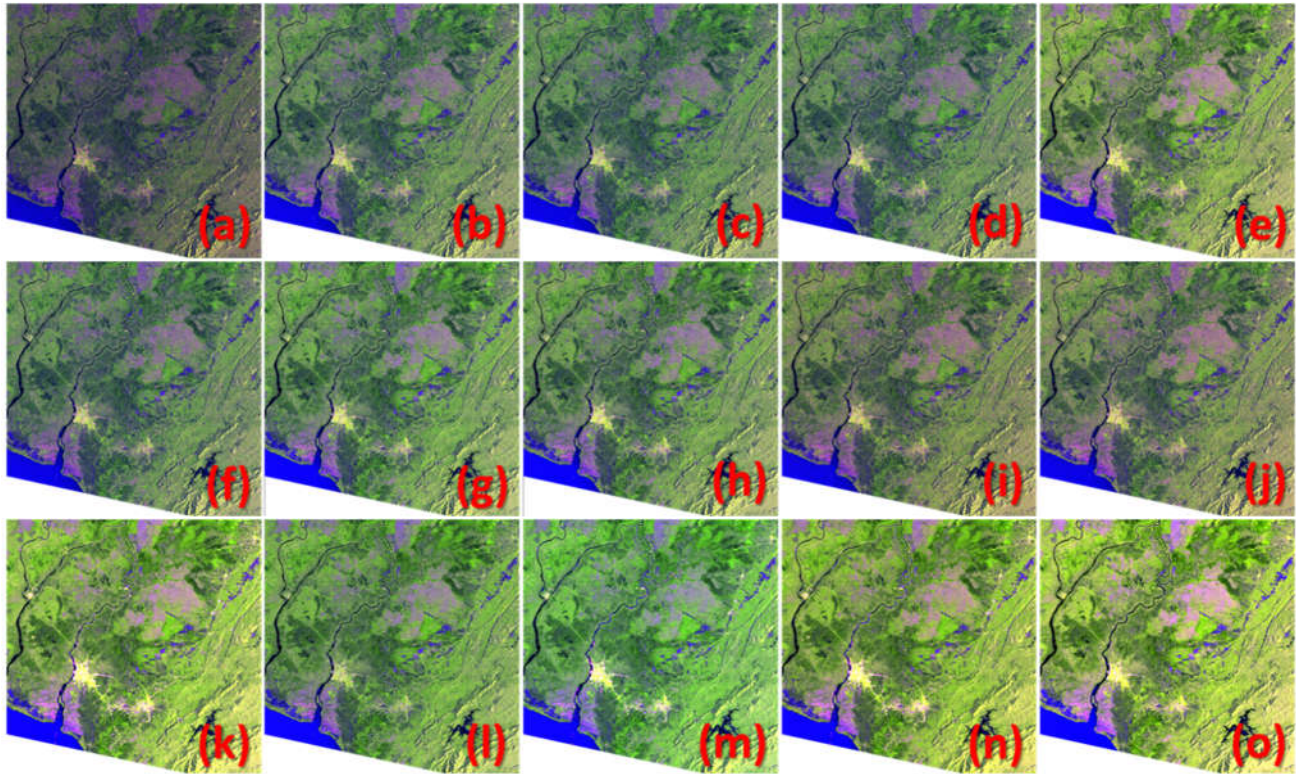


Fig. 8. Unfiltered Sentinel-1 imagery and speckle filtered Sentinel-1 imageries. (a) Original imagery (unfiltered); (b) Boxcar 3x3; (c) Frost 3x3; (d) Gamma Map 3x3; (e) IDAN; (f) Lee 3x3; (g) Lee Sigma 7x7 (target window 3x3); (h) Lee Sigma 7x7 (target window 5x5); (i) Median 3x3; (j) Refined Lee; (k) Boxcar 37x37; (l) Frost 49x49; (m) Gamma Map 37x37; (n) Lee 37x37; and (o) Median 37x37.

One of the main problems faced in speckle filtering is the execution process which is very time consuming. In this research we have used a workstation computer with a Core-i7 processor, 32 GB memory, and a fast PCIe Solid State Drive (SSD) hard drive. However, the process still feels quite heavy. The larger the processing window size, the heavier the process will be. Thus, large processing window sizes in speckle filtering may be very impractical for certain purposes. Furthermore, for the purposes of processing one full swath of Sentinel-1 imagery or larger, we do not recommend applying a processing window size that is large enough for computer specifications with less than 8 GB of memory and non-SSD hard drives.

In total, there were 71 times of speckle filtering processing applied in this study. Therefore, this would produce an output of 71 speckle filtered imageries. Of course, it is not possible to visually present all the filtering results in this paper. In Fig. 8, we only present speckle filtered image samples with the default settings from the SNAP application, plus 5 speckle filtered simulation results. More details about the number of the outputs can be seen in Table 1 and Table 2. Usually, speckle filtering performances were assessed using Root Mean Square Error (RMSE), Peak Signal to Noise Ratio (PSNR), Mean Structural Similarity Index Measure (MSSIM), Edge Preservation Index (EPI), or Equivalent Number of Looks (ENL). However, the accuracy assessment in this research is carried out using the Pearson Correlation Coefficient (PCC) or r values, which were calculated in pairs between DPSVI from speckle filtering results and vegetation biophysical information. This is because our target is to find the most accurate speckle filtering in the context of extracting vegetation biophysical information. Without paying too much attention to the presence of other features around the vegetation object.

Based on the results of the r calculation, it is clearly seen in Table 1 that for speckle filtering methods with the default parameter settings of the SNAP application, IDAN is able to provide the best results. Followed by Lee Sigma, Boxcar, Lee, Gamma Map, Refined Lee, Frost, and Median respectively. Therefore, for practical purposes in terms of extracting vegetation biophysical information, we could recommend IDAN or Lee Sigma. Indeed, speckle filtering using IDAN with its own default parameters is actually quite time consuming, compared to other methods. IDAN's best ability in this research is in line with the results of previous research²⁶. IDAN filter is able to reduce noise speckle significantly, but at the same time preserve fine detail and prevent blurring effect²⁶.

Table 1. PCC (r) values between DPSVI and vegetation biophysical information in each speckle filtering method.

| Speckle Filters | Parameters | Parameter Scoring | LAI | CWC | CCC | FVC | FAPAR |
|-------------------------------------|------------|-------------------|----------|----------|----------|----------|----------|
| Unfiltered | - | - | 0.296052 | 0.308913 | 0.263586 | 0.303591 | 0.311245 |
| Refined Lee | Default | - | 0.402843 | 0.419640 | 0.359107 | 0.413021 | 0.423679 |
| IDAN | Default | - | 0.560491 | 0.583778 | 0.500419 | 0.574348 | 0.589653 |
| Boxcar | 3x3* | 3 | 0.406172 | 0.422591 | 0.362794 | 0.416114 | 0.426334 |
| | 5x5 | 5 | 0.500568 | 0.520607 | 0.447841 | 0.512511 | 0.525250 |
| | 7x7 | 7 | 0.558434 | 0.580951 | 0.500135 | 0.571207 | 0.585663 |
| | 9x9 | 9 | 0.594633 | 0.619022 | 0.533044 | 0.607551 | 0.623243 |
| | 11x11 | 11 | 0.619269 | 0.645131 | 0.555676 | 0.631900 | 0.648513 |
| | 13x13 | 13 | 0.637250 | 0.664230 | 0.572488 | 0.649237 | 0.666527 |
| | 15x15 | 15 | 0.651037 | 0.678911 | 0.585718 | 0.662157 | 0.679973 |
| | 17x17 | 17 | 0.661868 | 0.690583 | 0.596318 | 0.672075 | 0.690300 |
| | 19x19 | 19 | 0.670407 | 0.699904 | 0.604730 | 0.679843 | 0.698342 |
| | 21x21 | 21 | 0.677627 | 0.707795 | 0.611872 | 0.686452 | 0.705157 |
| Frost | 3x3* | 3 | 0.403614 | 0.419940 | 0.360471 | 0.413520 | 0.423675 |
| | 5x5 | 5 | 0.489715 | 0.509239 | 0.438050 | 0.501473 | 0.513861 |
| | 7x7 | 7 | 0.541677 | 0.563361 | 0.485058 | 0.554118 | 0.567965 |
| | 9x9 | 9 | 0.574386 | 0.597673 | 0.514799 | 0.586902 | 0.601795 |
| | 11x11 | 11 | 0.596065 | 0.620611 | 0.534476 | 0.608524 | 0.624166 |
| | 13x13 | 13 | 0.610811 | 0.636241 | 0.547831 | 0.623213 | 0.639334 |
| | 15x15 | 15 | 0.620996 | 0.647026 | 0.557179 | 0.633248 | 0.649707 |
| | 17x17 | 17 | 0.628129 | 0.654575 | 0.563837 | 0.640159 | 0.656878 |
| | 19x19 | 19 | 0.633118 | 0.659860 | 0.568570 | 0.644933 | 0.661835 |
| | 21x21 | 21 | 0.636597 | 0.663570 | 0.571904 | 0.648247 | 0.665272 |
| Gamma Map | 3x3* | 3 | 0.405113 | 0.421601 | 0.361773 | 0.415049 | 0.425135 |
| | 5x5 | 5 | 0.496994 | 0.517203 | 0.444361 | 0.508978 | 0.521408 |
| | 7x7 | 7 | 0.550687 | 0.572854 | 0.492963 | 0.563386 | 0.577288 |
| | 9x9 | 9 | 0.586070 | 0.610063 | 0.525235 | 0.598720 | 0.613935 |
| | 11x11 | 11 | 0.613891 | 0.640094 | 0.550319 | 0.626397 | 0.642810 |
| | 13x13 | 13 | 0.634122 | 0.661834 | 0.568934 | 0.646281 | 0.663470 |
| | 15x15 | 15 | 0.648051 | 0.676678 | 0.582215 | 0.659451 | 0.677165 |
| | 17x17 | 17 | 0.658896 | 0.688350 | 0.592848 | 0.669302 | 0.687467 |
| | 19x19 | 19 | 0.667553 | 0.697679 | 0.601475 | 0.677001 | 0.695482 |
| | 21x21 | 21 | 0.674986 | 0.705630 | 0.609010 | 0.683636 | 0.702355 |
| Lee | 3x3* | 3 | 0.405462 | 0.421876 | 0.362130 | 0.415402 | 0.425554 |
| | 5x5 | 5 | 0.497538 | 0.517368 | 0.445103 | 0.509424 | 0.521971 |
| | 7x7 | 7 | 0.553706 | 0.575792 | 0.495919 | 0.566337 | 0.580530 |
| | 9x9 | 9 | 0.590880 | 0.614774 | 0.529834 | 0.603528 | 0.619005 |
| | 11x11 | 11 | 0.616842 | 0.642215 | 0.553616 | 0.629220 | 0.645608 |
| | 13x13 | 13 | 0.635423 | 0.662066 | 0.570844 | 0.647303 | 0.664352 |
| | 15x15 | 15 | 0.649455 | 0.677149 | 0.584167 | 0.660640 | 0.678217 |
| | 17x17 | 17 | 0.660473 | 0.689117 | 0.594870 | 0.670770 | 0.688803 |
| | 19x19 | 19 | 0.669288 | 0.698704 | 0.603586 | 0.678705 | 0.697074 |
| | 21x21 | 21 | 0.676754 | 0.706738 | 0.611098 | 0.685412 | 0.704030 |
| Median | 3x3* | 3 | 0.385276 | 0.401832 | 0.343492 | 0.394951 | 0.404840 |
| | 5x5 | 5 | 0.478489 | 0.499476 | 0.426043 | 0.491120 | 0.504198 |
| | 7x7 | 7 | 0.539055 | 0.562399 | 0.480472 | 0.552485 | 0.567756 |
| | 9x9 | 9 | 0.578467 | 0.603073 | 0.515982 | 0.592425 | 0.609261 |
| | 11x11 | 11 | 0.604744 | 0.630421 | 0.539959 | 0.618587 | 0.636504 |
| | 13x13 | 13 | 0.623689 | 0.650491 | 0.557393 | 0.637082 | 0.655747 |
| | 15x15 | 15 | 0.637261 | 0.664975 | 0.570080 | 0.650090 | 0.669203 |
| | 17x17 | 17 | 0.648717 | 0.676957 | 0.581104 | 0.660778 | 0.680255 |
| | 19x19 | 19 | 0.657876 | 0.686680 | 0.589989 | 0.669118 | 0.688895 |
| | 21x21 | 21 | 0.666001 | 0.695224 | 0.597863 | 0.676586 | 0.696588 |
| Lee Sigma (Target Window Size 3x3*) | 5x5 | 5 | 0.458273 | 0.478633 | 0.410470 | 0.467116 | 0.477632 |
| | 7x7* | 7 | 0.492558 | 0.515541 | 0.441533 | 0.501112 | 0.512294 |
| | 9x9 | 9 | 0.511214 | 0.535856 | 0.458516 | 0.519460 | 0.531077 |
| | 11x11 | 11 | 0.522779 | 0.548637 | 0.469182 | 0.530513 | 0.542501 |
| | 13x13 | 13 | 0.530884 | 0.557580 | 0.476849 | 0.537972 | 0.550220 |
| | 15x15 | 15 | 0.537240 | 0.564687 | 0.483119 | 0.543532 | 0.556024 |
| Lee Sigma (Target Window Size 5x5) | 7x7* | 7 | 0.447942 | 0.468408 | 0.401217 | 0.455599 | 0.465458 |
| | 9x9 | 9 | 0.479107 | 0.502305 | 0.429655 | 0.485929 | 0.496351 |
| | 11x11 | 11 | 0.495054 | 0.520080 | 0.444272 | 0.501220 | 0.512074 |
| | 13x13 | 13 | 0.505303 | 0.531432 | 0.453770 | 0.510875 | 0.521946 |
| | 15x15 | 15 | 0.512040 | 0.539001 | 0.460174 | 0.516981 | 0.528226 |
| | 17x17 | 17 | 0.516941 | 0.544539 | 0.465053 | 0.521155 | 0.532538 |
| | 19x19 | 19 | 0.520409 | 0.548459 | 0.468659 | 0.524069 | 0.535504 |

* SNAP default window processing sizes

Henceforward, the results of testing the processing window size up to 21x21 show that Boxcar with a processing window size of 21x21 is the best speckle filtering method, as shown in Table 1. The ability of Boxcar with a 21x21 window applies to all vegetation biophysical information parameters tested in this study, namely LAI, CWC, CCC, FVC, and FAPAR. Boxcar's abilities are followed by Lee, Gamma Map, Median, and Frost respectively. Each with a processing window size of 21x21, and overall, with r values of 0.6s to 0.7s.

Most comparative research of speckle filtering methods generally only presents speckle filtering trials at default settings, for example Lee with a processing window size of 3x3, or setting some variations of processing window sizes. This is what distinguishes this research from previous research. Because in this research, if no values of r were found that reach 0.8, then simulations would be implemented to determine the most optimal processing window sizes for the extraction of certain biophysical vegetations. Of course, not all speckle filtering methods tested in this research can be included in the simulation, because some speckle filtering methods set a fixed processing window size or limit the processing window to a certain size. In fact, from the test results of all speckle filtering methods up to a processing window size of 21x21, no r value of 0.8 was found. Therefore, the decision is to do a simulation or modeling using the regression method, to estimate what the most optimal window size is so that an r value of 0.8 can be achieved for each speckle filtering method, on each vegetation biophysical information parameter.

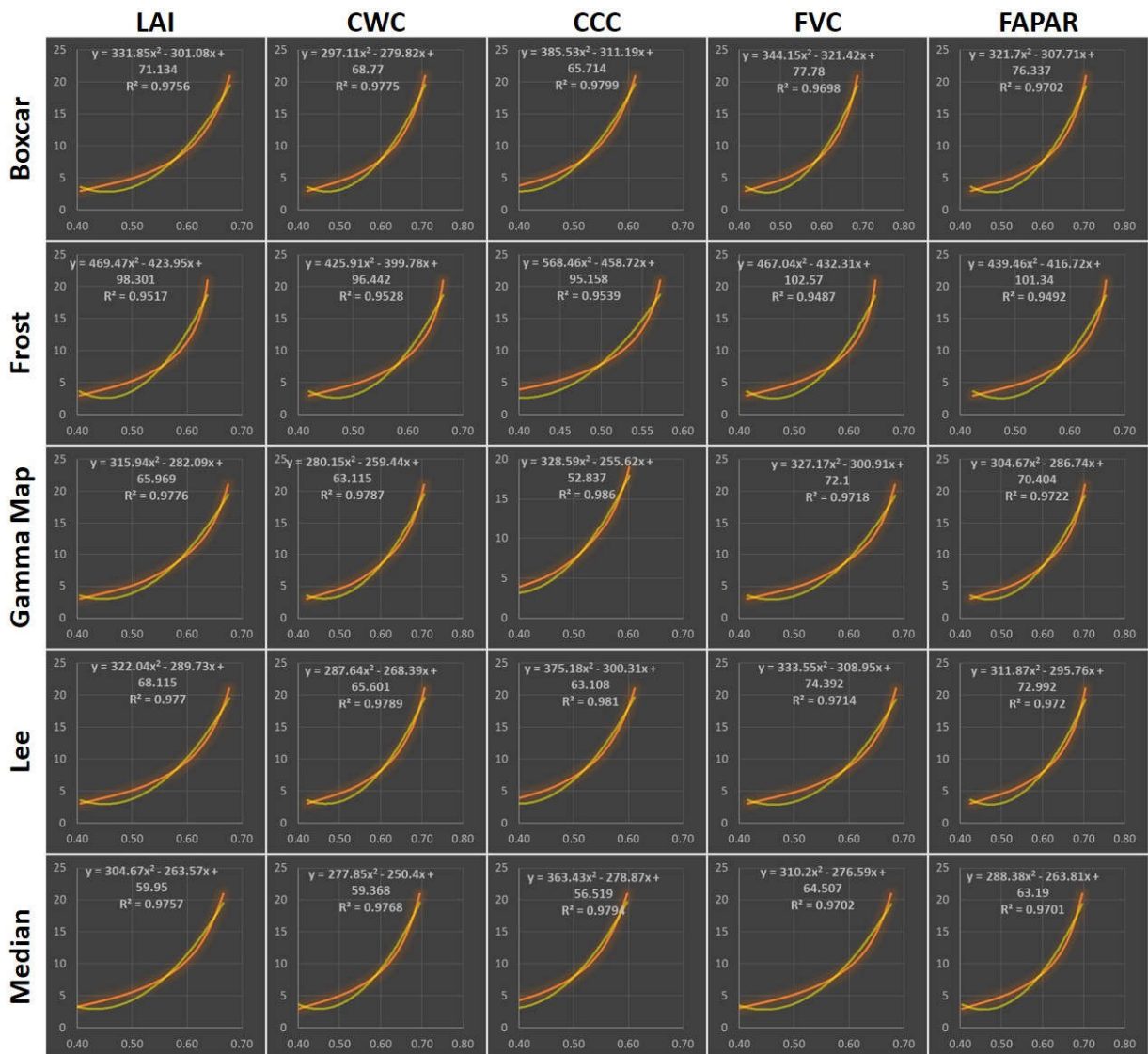


Fig. 9. Regression models to predict the most optimal processing window sizes.

Fig. 9 shows the simulation results of processing window sizes to reach r values up to 0.8. The entire speckle filtering method for each vegetation biophysical information parameter shows a polynomial (quadratic) correlation with increasing processing window sizes. In Fig. 9, we only present the test regression models with the highest correlation coefficients (r^2). Because it would be too much if we had to display graphs for all the regression models tested in this study. Overall r^2 shows a value of 0.9 more, this means between the increase in processing window sizes with accuracy (r). However, since the correlations are quadratic, it could be predicted that at some point the values of r will be saturated, even though the processing window sizes in speckle filtering are enlarged. In other words, increasing the processing window sizes to certain sizes will no longer be able to significantly increase the accuracy of the speckle filtering methods.

In order to assess the simulation results of processing window sizes, we sampled one of the vegetation biophysical information parameters, namely FAPAR, to be tested on five speckle filtering methods, namely Boxcar, Frost, Gamma Map, Lee, Median. Each with the window size of the simulation results as shown in Table 1, in the FAPAR column. Boxcar, Gamma Map, Lee, and Median, were tested using a size of 37x37, while Frost was tested using a size of 49x49. These 37x37 and 49x49 measures were calculated using the quadratic regression models in Fig. 9, specifically for FAPAR. If the quadratic regression calculation processes produce a number that is not odd, then the result of the calculation process would be rounded up to the odd number above it. For example, one calculation process results in the number 36 or 36.24, it would be rounded to 37. This is because the processing window sizes in speckle filtering or image filtering in general must be odd numbers, such as 37x37. Of course, the size of 37x37 let alone 49x49 is the size of the speckle filtering window which is quite large, so it will require quite high computer resources. Furthermore, it appears that overall, to reach an r value of 0.8, processing window sizes ranging from 35x35 to 93x93 are required for certain vegetation biophysical information parameters.

Table 2. Estimated processing window sizes for each method of speckle filtering and vegetation biophysical information to reach a PCC value of 0.8.

| | LAI | CWC | CCC | FVC | FAPAR |
|-----------|---------|---------|---------|---------|---------|
| Boxcar | 43 x 43 | 35 x 35 | 65 x 65 | 41 x 41 | 37 x 37 |
| Frost | 61 x 61 | 49 x 49 | 93 x 93 | 57 x 57 | 49 x 49 |
| Gamma Map | 43 x 43 | 35 x 35 | 59 x 59 | 41 x 41 | 37 x 37 |
| Lee | 43 x 43 | 35 x 35 | 63 x 63 | 41 x 41 | 37 x 37 |
| Median | 45 x 45 | 37 x 37 | 67 x 67 | 43 x 43 | 37 x 37 |

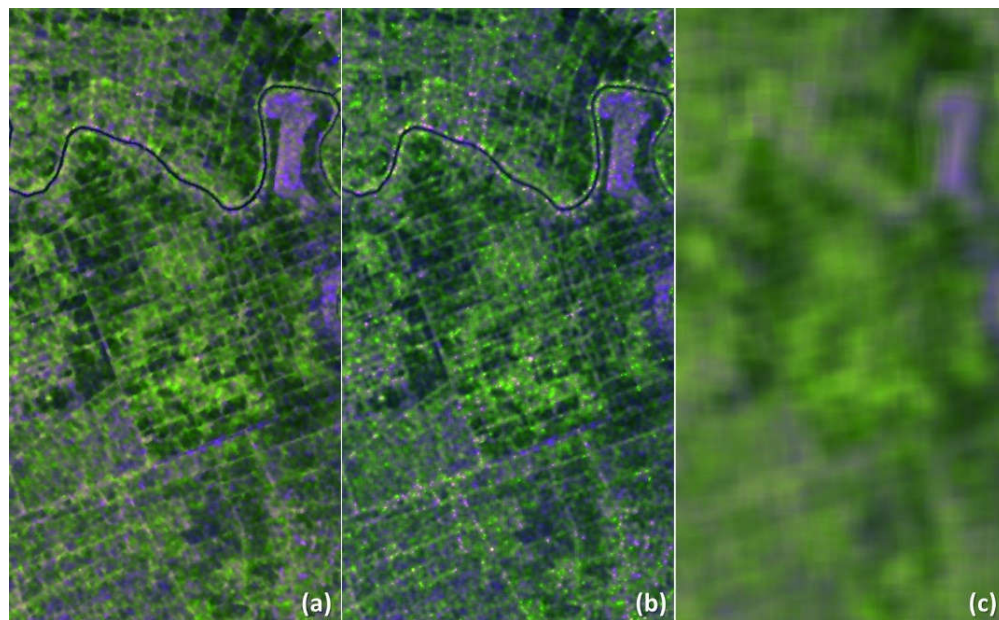


Fig. 10. Visual comparison between (a) IDAN, (b) Lee Sigma 7x7 (target window size 3x3), and (c) Boxcar 37x37.

The results of the speckle filtering using the simulated window sizes were then retested using PCC. The test results show that the r value for Boxcar is 0.735194, the r value for Frost is 0.668937, the r value for Gamma Map is 0.730305, the r value for Lee is 0.733073, and the r value for Median is 0.730752. Even though the r values increase after the processing window sizes are enlarged by simulation, however the results of this assessment are below expectations, where the resulting r values expected to be around 0.8. Our prediction is that this is due to the insufficient sample size of the speckle filtering window in the construction of the regression models. As a result, the regression models produced in this research are overestimated. In the construction of regression models there are only 10 samples, namely from window sizes 3x3 to 21x21. In fact, to build an objective regression model, at least 30 data samples are needed. It may be necessary to further study at least to prepare a sufficient number of samples of speckle filtering window sizes.

In addition to requiring adequate computer hardware, there are other implications that will be experienced by SAR images when the processing window size is large enough. Among them are the decrease in the spatial resolution of the image and the blur effect on the image, as shown in Fig. 10. So that although on the one hand it is advantageous, namely by increasing the correlation value or accuracy, but this can also be detrimental. Because we will lose certain details in the image. Thus, the use of a sufficiently large processing window in speckle filtering must also be carefully considered. The capabilities of IDAN and Lee Sigma are almost equal, if each with default settings. Both are able to reduce speckle effects significantly, while maintaining detail on the image well. However, there is one drawback to Lee Sigma. Namely having the presence of bright spots on certain features, as shown in Fig. 10. Where this is not experienced by the IDAN filter. So that in this case IDAN is indeed superior compared with Lee Sigma, both statistically and visually. The similarity between IDAN and Lee Sigma is that for IDAN the processing window size is fixed, so it cannot be changed, and for Lee Sigma, the processing window size setting is very limited.

5. CONCLUSIONS

In this research, we focus more on presenting a comparison of the capabilities of several speckle filtering methods to extract various vegetation biophysical information parameters. Without having to review further the fundamental concepts of each speckle filtering method. The results of the research show that in setting the default parameters using SNAP software, IDAN and Lee Sigma are able to provide the best performance. However, these two filters are less flexible in setting processing window sizes. When the processing window sizes are set to 21x21, the Boxcar method and Lee's method give the best results, with the PCC values ranging from 0.6s to 0.7s. Even when processing window sizes are simulated to reach a PCC value of 0.8, Boxcar still delivers the best output. Despite the fact that the PCC value of 0.8 was never achieved in this research, this was due to the limited number of samples in the simulation. Of course, with the consequence of decreasing the spatial resolution of the image and losing certain details on the image.

ACKNOWLEDGEMENTS

This research was funded by the Center for Geospatial Information Infrastructure Development (PPIIG) of Universitas Lambung Mangkurat, Banjarbaru, Indonesia. We thank the European Space Agency (ESA) which has provided Sentinel-1 SAR imagery, Sentinel-2 MSI imagery, and SNAP software for free. And also, to the Geospatial Information Laboratory, Faculty of Forestry, Universitas Lambung Mangkurat, which has facilitated digital imagery processing in this research.

REFERENCES

- [1] Arienzo, A., Argenti, F., Alparone, L. and Gherardelli, M., "Accurate Despeckling and Estimation of Polarimetric Features by Means of a Spatial Decorrelation of the Noise in Complex PolSAR Data," *Remote Sensing* 12 (2), 331 (2020).
- [2] Attema E. P. W. and Ulaby, F. T., "Vegetation modeled as a water cloud," *Radio Science* 13 (2), 357-364 (1978).
- [3] Baghdadi, N., El Hajj, M., Zribi, M. and Bousbih, S., "Calibration of the Water Cloud Model at C-Band for Winter Crop Fields and Grasslands," *Remote Sensing* 9 (9), 969 (2017).
- [4] Bai, X., He, B., Li, X., Zeng, J., Wang, X., Wang, Z., Zeng, Y. and Su, Z., "First Assessment of Sentinel-1A Data for Surface Soil Moisture Estimations Using a Coupled Water Cloud Model and Advanced Integral Equation Model over the Tibetan Plateau," *Remote Sensing* 9 (7), 714 (2017).

- [5] Bao, Y., Lin, L., Wu, S., Kwal Deng, K. A. and Petropoulos, G. P., "Surface soil moisture retrievals over partially vegetated areas from the synergy of Sentinel-1 and Landsat 8 data using a modified water-cloud model," *International Journal of Applied Earth Observation and Geoinformation* 72, 76-85 (2018).
- [6] Baraldi, A. and Parmigiani, F., "A Refined Gamma MAP SAR Speckle Filter with Improved Geometrical Adaptivity," *IEEE Transactions on Geoscience and Remote Sensing* 33 (5), 1245-1257 (1995).
- [7] Bouchemakh, L., Smara, Y., Boutarfa, S. and Hamadache, Z., "A Comparative Study of Speckle Filtering In Polarimetric Radar SAR Images," 2008 3rd International Conference on Information and Communication Technologies: From Theory to Applications, 1-6 (2008).
- [8] Brown, L. A., Fernandes, R., Djamai, N., Meier, C., Gobron, N., Morris, H., Canisius, F., Bai, G., Lerebourg, C., Lanconelli, C., Clerici, M. and Dash, J., "Validation of baseline and modified Sentinel-2 Level 2 Prototype Processor leaf area index retrievals over the United States," *ISPRS Journal of Photogrammetry and Remote Sensing* 175, 71-87 (2021).
- [9] Djamai, N., Fernandes, R., Weiss, M., McNairn, H. and Goïta, K., "Validation of the Sentinel Simplified Level 2 Product Prototype Processor (SL2P) for mapping cropland biophysical variables using Sentinel-2/MSI and Landsat-8/OLI data," *Remote Sensing of Environment* 225, 416-430 (2019).
- [10] Farage, G., Foucher, S. and Benie, G., "Comparison of PolSAR Speckle Filtering Techniques," 2006 IEEE International Symposium on Geoscience and Remote Sensing, 1760-1763 (2006).
- [11] Foucher, S. and López-Martínez, C., "Analysis, Evaluation, and Comparison of Polarimetric SAR Speckle Filtering Techniques," *IEEE Transactions on Image Processing* 23, 1751-1764 (2014).
- [12] Frost, V.S., Stiles, J. A., Shanmugan, K. S. and Holtzman, J., "A Model for Radar Images and Its Application to Adaptive Digital Filtering of Multiplicative Noise," *IEEE Transactions on Pattern Analysis and Machine Intelligence* 4 (2), 157-165 (1982).
- [13] Garioud, A., Valero, S., Giordano, S. and Mallet, C., "Recurrent-based regression of Sentinel time series for continuous vegetation monitoring," *Remote Sensing of Environment* 263, 112419 (2021).
- [14] Giri Ananto, W. H., Putri, A. F. S., Hadi, H. A., Hanum, D. N., Wiryanan, W. K. P., Prabaswara, R. R. and Arjasakusuma, S., "Performance of various speckle filter methods in modelling forest aboveground biomass using Sentinel-1 data: case study of Barru Regency, South Sulawesi," *Proceedings of SPIE* 11311, Sixth Geoinformation Science Symposium, 113110P (21 November 2019).
- [15] Graham, A. J. and Harris, R., "Extracting biophysical parameters from remotely sensed radar data: a review of the water cloud model," *Progress in Physical Geography: Earth and Environment* 27 (2), 217-229 (2003).
- [16] Kang, Y., Ozdogan, M., Gao, F., Anderson, M. C., White, W. A., Yang, Y., Yang, Y. and Erickson, T. A., "A data-driven approach to estimate leaf area index for Landsat images over the contiguous US," *Remote Sensing of Environment* 258, 112383 (2021).
- [17] Kganyago, M., Mhangara, P., Alexandridis, T., Laneve, G., Ovakoglou, G. and Mashiyi, N., "Validation of sentinel-2 leaf area index (LAI) product derived from SNAP toolbox and its comparison with global LAI products in an African semi-arid agricultural landscape," *Remote Sensing Letters* 11 (10), 883-892 (2020).
- [18] Lang, S., Lin, C. Y., Liu, J., Wong, N., Kwok-Hay So, H., "A comparison of SAR image speckle filters," *Proceedings of SPIE* 7498, MIPPR 2009: Remote Sensing and GIS Data Processing and Other Applications, 749804 (30 October 2009).
- [19] Lee, J. S., "Speckle analysis and smoothing of synthetic aperture radar images," *Computer Graphics and Image Processing* 17 (1), 1981, 24-32 (1981).
- [20] Lee, J. S., "A simple speckle smoothing algorithm for synthetic aperture radar images," *IEEE Transactions on System, Man, and Cybernetics SMC-13* (1), 85-89, (1983).
- [21] Lee, J. S., "Digital image smoothing and the sigma filter," *Computer Vision, Graphics, and, Image Processing* 24 (2), 255-269, (1983).
- [22] Lee, J. S., Jurkevich, J., Dewaele, P., Wambacq, P. and Oosterlinck, A., "Speckle filtering of synthetic aperture radar images: A review," *Remote Sensing Reviews* 8 (4), 313-340 (1994).
- [23] Lee, J. S., Grunes, M. R. and de Grandi, G., "Polarimetric SAR speckle filtering and its implication for classification," *IEEE Transactions on Geoscience and Remote Sensing* 37 (5), 2363-2373 (1999).
- [24] Mandal, D., Kumar, V., Ratha, D., Dey, S., Bhattacharya, A., Lopez-Sanchez, J. M., McNairn, H. and Rao, Y. S., "Dual polarimetric radar vegetation index for crop growth monitoring using sentinel-1 SAR data," *Remote Sensing of Environment* 247, 111954 (2020).

- [25] Mandal D., Kumar, V., Lopez-Sanchez, J. M., Bhattacharya, A., McNairn, H. and Rao, Y. S., "Crop biophysical parameter retrieval from Sentinel-1 SAR data with a multi-target inversion of Water Cloud Model," *International Journal of Remote Sensing* 41 (14), 5503-5524 (2020).
- [26] Medasani, S. and Reddy, G. U., "Analysis and Evaluation of Speckle Filters for Polarimetric Synthetic Aperture Radar (PolSAR) Data," *International Journal of Applied Engineering Research* 12 (15), 4916-4927 (2017).
- [27] Meyer, F., "Spaceborne Synthetic Aperture Radar: Principles, Data Access, and Basic Processing Techniques," in Flores-Anderson, A. I., Herndon, K. E., Thapa, R. B., and Cherrington, E., (eds.), [The Synthetic Aperture Radar (SAR) Handbook: Comprehensive Methodologies for Forest Monitoring and Biomass Estimation], SERVIR Global Science, 21-63 (2019).
- [28] Morandeira, N. S., Grimson, R. and Kandus, P., "Assessment of SAR speckle filters in the context of object-based image analysis," *Remote Sensing Letters* 7 (2), 150-159 (2016).
- [29] Otsu, N., "A Threshold Selection Method from Gray-level Histograms," *IEEE Transactions on Systems, Man, and Cybernetics* 9, 62-69 (1979).
- [30] Periasamy, S., "Significance of dual polarimetric synthetic aperture radar in biomass retrieval: An attempt on Sentinel-1," *Remote Sensing of Environment* 217, 537-549 (2018).
- [31] Potapov, P., Tyukavina, A., Turubanova, S., Talero, Y., Hernandez-Serna, A., Hansen, M.C., Saah, D., Tenneson, K., Poortinga, A., Aekakkararungroj, A., Chishtie, F., Towashiraporn, P., Bhandari, B., Aung, K.S. and Nguyen, Q.H., "Annual continuous fields of woody vegetation structure in the Lower Mekong region from 2000-2017 Landsat time-series," *Remote Sensing of Environment* 232, 111278 (2019).
- [32] Ramesh, J. P., Badruddin, S.S. and Waghji, K. P., "Comparative Study of Gaussian and Box-Car Filter of TerraSAR-X Data Image using Pol-SAR for Speckle Noise Reduction," *International Journal of Recent Scientific Research* 9 (5), 26977-26980 (2018).
- [33] Richards, J. A., [Remote Sensing with Imaging Radar], Springer-Verlag, Berlin Heidelberg, 120 (2009).
- [34] Rouse, J. W., Haas, R. H., Schell, J. A. and Deering, D. W., "Monitoring vegetation systems in the Great Plains with ERTS," *Third ERTS Symposium NASA SP-351 I*, 309-317 (1973).
- [35] Santoso, A.W., Bayuaji, L., Sze, L. T., Lateh, H. and Zain, J. M., "Comparison of Various Speckle Noise Reduction Filters on Synthetic Aperture Radar Image," *International Journal of Applied Engineering Research* 11 (15), 8760-8767 (2016).
- [36] Schneider, C. A., Rasband, W. S. and Eliceiri, K. W., "NIH Image to ImageJ: 25 Years of Image Analysis," *Nature Methods* 9 (7), 671-675 (2012), PMID 22930834.
- [37] Schindelin, J., Rueden, C. T., Hiner, M. C. and Eliceiri, K. W., "The ImageJ Ecosystem: An open Platform for Biomedical Image Analysis," *Molecular Reproduction and Development*, (2015), PMID 26153368.
- [38] Sullivan, R., "Synthetic Aperture Radar," in Skolnik, M. I. (Editor in Chief), [Radar Handbook, Third Edition], The McGraw-Hill Companies, New York Chicago San Francisco Lisbon London Madrid Mexico City Milan New Delhi San Juan Seoul Singapore Sydney Toronto, 17.19-17.20 (2008).
- [39] Sun, S., Liu, R., Yang, C., Zhou, H., Zhao, J. and Ma, J., "Comparative study on the speckle filters for the very high-resolution polarimetric synthetic aperture radar imagery," *Journal of Applied Remote Sensing* 10 (4), 045014 (2016).
- [40] Vasile, G., Trouvé, E., Lee, J.S., and Buzuloiu, V., "Intensity-Driven Adaptive-Neighborhood Technique for Polarimetric and Interferometric SAR Parameters Estimation," *IEEE Transactions on Geoscience and Remote Sensing* 44 (6), 1609-1621 (2006).
- [41] Wang, J., "Pearson correlation coefficient," in Dubitzky W., Wolkenhauer O., Cho KH., Yokota H. (eds) [Encyclopedia of Systems Biology], Springer, New York, (2013).
- [42] Weiss, M. and Baret, F., S2ToolBox Level 2 products: LAI, FAPAR, FCOVER Version 1.1, (2016), https://step.esa.int/docs/extra/ATBD_S2ToolBox_L2B_V1.1.pdf.
- [43] Yadav, V. P., Prasad, R., Bala, R. and Srivastava, P. K., "Assessment of red-edge vegetation descriptors in a modified water cloud model for forward modelling using Sentinel-1A and Sentinel-2 satellite data," *International Journal of Remote Sensing* 42 (3), 794-804 (2021).
- [44] Yang, P., Verhoef, W., Prikaziuk, E. and van der Tol, C., "Improved retrieval of land surface biophysical variables from time series of Sentinel-3 OLCI TOA spectral observations by considering the temporal autocorrelation of surface and atmospheric properties," *Remote Sensing of Environment* 256, 112328 (2021).
- [45] Yommy, A. S., Liu, R. and Wu, A. S., "SAR Image Despeckling Using Refined Lee Filter," 2015 7th International Conference on Intelligent Human-Machine Systems and Cybernetics, 260-265 (2015).

PROCEEDINGS OF SPIE

SPIDigitalLibrary.org/conference-proceedings-of-spie

Front Matter: Volume 12082

, "Front Matter: Volume 12082," Proc. SPIE 12082, Seventh Geoinformation Science Symposium 2021, 1208201 (22 December 2021); doi: 10.1117/12.2625912

SPIE.

Event: Seventh Geoinformation Science Symposium (GSS 2021), 2021, Yogyakarta, Indonesia

PROCEEDINGS OF SPIE

Seventh Geoinformation Science Symposium 2021

**Sandy Budi Wibowo
Pramaditya Wicaksono**
Editors

**25–28 October 2021
Yogyakarta, Indonesia**

Organized by
Department of Geographic Information Science, Faculty of Geography,
Universitas Gadjah Mada (Indonesia)
Indonesian Geographers Association

Sponsored by
Faculty of Geography, Universitas Gadjah Mada (Indonesia)

Published by
SPIE

Volume 12082

Proceedings of SPIE 0277-786X, V. 12082

SPIE is an international society advancing an interdisciplinary approach to the science and application of light.

Seventh Geoinformation Science Symposium 2021, edited by Sandy Budi Wibowo,
Pramaditya Wicaksono, Proc. of SPIE Vol. 12082, 1208201
© 2021 SPIE · 0277-786X · doi: 10.1117/12.2625912

Proc. of SPIE Vol. 12082 1208201-1

The papers in this volume were part of the technical conference cited on the cover and title page. Papers were selected and subject to review by the editors and conference program committee. Some conference presentations may not be available for publication. Additional papers and presentation recordings may be available online in the SPIE Digital Library at SPIDigitalLibrary.org.

The papers reflect the work and thoughts of the authors and are published herein as submitted. The publisher is not responsible for the validity of the information or for any outcomes resulting from reliance thereon.

Please use the following format to cite material from these proceedings:
Author(s), "Title of Paper," in *Seventh Geoinformation Science Symposium 2021*, edited by Sandy Budi Wibowo, Pramaditya Wicaksono, Proc. of SPIE 12082, Seven-digit Article CID Number (DD/MM/YYYY); (DOI URL).

ISSN: 0277-786X
ISSN: 1996-756X (electronic)

ISBN: 9781510650404
ISBN: 9781510650411 (electronic)

Published by
SPIE
P.O. Box 10, Bellingham, Washington 98227-0010 USA
Telephone +1 360 676 3290 (Pacific Time)
SPIE.org
Copyright © 2021 Society of Photo-Optical Instrumentation Engineers (SPIE).

Copying of material in this book for internal or personal use, or for the internal or personal use of specific clients, beyond the fair use provisions granted by the U.S. Copyright Law is authorized by SPIE subject to payment of fees. To obtain permission to use and share articles in this volume, visit Copyright Clearance Center at copyright.com. Other copying for republication, resale, advertising or promotion, or any form of systematic or multiple reproduction of any material in this book is prohibited except with permission in writing from the publisher.

Printed in the United States of America by Curran Associates, Inc., under license from SPIE.

Publication of record for individual papers is online in the SPIE Digital Library.

SPIE. DIGITAL LIBRARY
SPIDigitalLibrary.org

Paper Numbering: A unique citation identifier (CID) number is assigned to each article in the Proceedings of SPIE at the time of publication. Utilization of CIDs allows articles to be fully citable as soon as they are published online, and connects the same identifier to all online and print versions of the publication. SPIE uses a seven-digit CID article numbering system structured as follows:

- The first five digits correspond to the SPIE volume number.
- The last two digits indicate publication order within the volume using a Base 36 numbering system employing both numerals and letters. These two-number sets start with 00, 01, 02, 03, 04, 05, 06, 07, 08, 09, 0A, 0B ... 0Z, followed by 10-1Z, 20-2Z, etc. The CID Number appears on each page of the manuscript.

Contents

BASIC REMOTE SENSING

- 12082 02 **Sharpening of Sentinel-2 imagery for updating thematic layer of base maps** [12082-41]
- 12082 03 **Comparison of topographic correction methods on SPOT-6/7 multispectral data in Indonesia: an initial evaluation in hilly to undulating area** [12082-43]
- 12082 04 **Sentinel-2A MSI and Landsat-8 OLI spectral reflectance comparison in tropical environments: a preliminary research for data fusion** [12082-12]

GEOSPATIAL ARTIFICIAL INTELLIGENCE

- 12082 05 **Deep neural network regression for estimating land surface temperature at 10 meter spatial resolution using Landsat-8 and Sentinel-2 data** [12082-19]
- 12082 06 **Mapping built-up land and settlements: a comparison of machine learning algorithms in Google Earth engine** [12082-47]
- 12082 07 **Assessment of image segmentation and deep learning for mapping paddy fields using Worldview-3 in Magelang, Central Java Provinces, Indonesia** [12082-50]
- 12082 08 **Application of random forest algorithm to Sentinel-1 for plantation detection: case study of Tesso Nilo ecosystem** [12082-34]

GEOSPATIAL APPLICATION FOR AGRICULTURAL STUDY

- 12082 09 **Agricultural drought identification based on Soil Moisture Index (SMI) during 2019 Indian Ocean Dipole (IOD) in Bekasi Regency** [12082-59]
- 12082 0A **Spatial and temporal analysis of drought in rice fields using Normalized Difference Drought Index (NDDI) in Indramayu Regency** [12082-16]
- 12082 0B **Identification of paddy fields based on temporal phase using Spectral Angle Mapper (SAM) on Landsat-8 OLI** [12082-40]
- 12082 0C **Mapping the sensitivity of agricultural land: a study of agricultural land conversion In Yogyakarta urban area** [12082-52]

APPLIED REMOTE SENSING FOR ATMOSPHERIC STUDY

- 12082 0D **Attenuation correction effects on quantitative precipitation estimation (QPE) at Sidoarjo weather radar** [12082-24]
- 12082 0E **Analysis of convective cloud presence surrounding whirlwind events in Yogyakarta, Indonesia** [12082-21]
- 12082 0F **Analysis of extreme rainfall distribution and tropical cyclone impact in Yogyakarta, Indonesia** [12082-20]

APPLIED REMOTE SENSING FOR MARINE STUDY

- 12082 0G **Live and dead coral cover mapping using PlanetScope image around Mandangin Island, Madura, Indonesia** [12082-42]
- 12082 0H **Chlorophyll-a and total suspended matter retrieval and comparison of C2RCC neural network algorithms on Landsat 8 data over Wangi-Wangi Island, Indonesia** [12082-18]
- 12082 0I ***Sardinella lemuru* abundance in Bali Strait: IOD or ENSO** [12082-39]

APPLIED REMOTE SENSING FOR URBAN STUDY I

- 12082 0J **Identification of spatial ecological sensitivity in Banyumas region** [12082-10]
- 12082 0K **The development of urban heat island in Jakarta based on satellite observation** [12082-28]

APPLIED REMOTE SENSING FOR URBAN STUDY II

- 12082 0L **Mapping and analysis of built-up area development in Batam City from 2000 to 2015** [12082-1]
- 12082 0M **Estimating population of Java Island based on nighttime lights data** [12082-2]
- 12082 0N **Analysis spatial pattern of urban growth using remote sensing data: a study in Purwokerto, Central Java, Indonesia** [12082-11]
- 12082 0O **Analysis of the relationships between land surface temperature and spectral indices pre- and during pandemic using Landsat-8 images (case study: Gerbangkertosusila)** [12082-30]

APPLIED REMOTE SENSING FOR VEGETATION STUDY I

- 12082 0P **Water quality modeling in mangrove forest area due to anthropogenic waste as a prevention of global warming utilizing remote sensing satellite data** [12082-33]
- 12082 0Q **Estimation of above ground carbon stock using multiple vegetation index on Sentinel-2 imagery (case study: Samarinda, East Kalimantan)** [12082-22]
- 12082 0R **Aboveground mangrove carbon stock mapping using WorldView-2 imagery** [12082-36]
- 12082 0S **The effect of atmospheric and topographic corrections on the vegetation density mapping using several vegetation indices: a case study in Arjuno-Welirang volcanoes, East Java** [12082-54]

APPLIED REMOTE SENSING FOR VEGETATION STUDY II

- 12082 0T **Comparing several pixel-based classification methods for vegetation structural composition mapping using Sentinel 2A imagery in Salatiga area, Central Java** [12082-55]
- 12082 0U **An object-based approach for vegetation and non-vegetation discrimination using WorldView-2 image** [12082-38]
- 12082 0V **On finding optimal speckle filtering for extraction of vegetation biophysical information using Sentinel-1 SAR imagery** [12082-5]
- 12082 0W **Estimated change in the percentage of vegetation cover after the eruption of Mount Agung, Bali in 2017** [12082-15]

GEOGRAPHIC INFORMATION SYSTEMS FOR HYDROLOGY

- 12082 0X **Flood control management recommendation of Citarum Hilir sub-watersheds using remote sensing and geographic information system approach** [12082-48]
- 12082 0Y **Assessment of aquifer susceptibility to land subsidence due to groundwater over-exploitation in Yogyakarta-Sleman groundwater basin** [12082-7]
- 12082 0Z **Water catchment critical level identification for revitalization planning of the Luk Ulo watershed, Central Java, Indonesia** [12082-31]

GEOGRAPHIC INFORMATION SYSTEMS FOR HAZARD STUDY

- 12082 10 **Spatio-temporal analysis of the direction of Merapi volcanic eruption in 2010 and 2020** [12082-32]
- 12082 11 **GIS for geomorphological analysis: facies of Merapi Volcano and morphometry of Gendol River** [12082-49]

GEOGRAPHIC INFORMATION SYSTEMS FOR HEALTH STUDY

- 12082 12 **Spatiotemporal analysis using Google Earth Engine: an evaluation of Covid-19 emergency response mobility policies in Java island, Indonesia** [12082-27]
- 12082 13 **Mapping of regional vulnerability to determine malaria using physical, climate, and socio-demographic variables in Purworejo Regency, Central Java** [12082-44]

GEOGRAPHIC INFORMATION SYSTEMS MODELLING

- 12082 14 **Potential development of spatial dynamics modeling research in Indonesia for environmental carrying capacity analysis** [12082-6]
- 12082 15 **The role of GIS and remote sensing for population mobility mapping** [12082-13]

CARTOGRAPHY AND GEOVISUALIZATION

- 12082 16 **Geotemporal analysis and topic modelling of Twitter data: study in nine big city areas of Indonesia** [12082-37]

On Finding Optimal Speckle Filtering for Extraction of Vegetation Biophysical Information Using Sentinel-1 SAR Imagery

The 7th Geoinformation Science Symposium 2021

“Rise from Adversity using Geospatial Technology”

“Virtual Conference, 25 - 28 October 2021”

Presented by:

Syamani D. Ali*, Abdi Fithria, Adi Rahmadi, Arfa Agustina Rezekiah

*Corresponding email: syamani.fhut@ulm.ac.id



Faculty of Forestry
Universitas Lambung Mangkurat
<http://fahutan.ulm.ac.id>



Center for Geospatial Information Infrastructure Development (PPIIG)
Universitas Lambung Mangkurat
<http://ppiig.ulm.ac.id>

Introduction

- The optical imageries such as Sentinel-2 MSI have a major drawback, which is that they are very sensitive to atmospheric disturbances.
- Despite the fact that SAR imagery such as Sentinel-1 has advantages over optical imageries in terms of minimizing atmospheric effects, it has one major drawback, namely the presence of speckle effects.
- For tropical areas such as Indonesia, which always experience the presence of atmospheric disturbances such as clouds, monitoring the vegetation biophysical information throughout time continuously is a special challenge. For the reason that the temporal resolution of optical sensors is strongly affected by cloud cover, resulting in significant missing information.
- The use of complementary acquisitions, such as Synthetic Aperture Radar (SAR) data, opens the door to the development of new multi-sensor methodologies aiming at the reconstruction of missing information.
- Recently, there are many SAR imaging technologies that have been developed, which can be used to extract vegetation biophysical information. Such as the Advanced Land Observing Satellite-Phased Array L-band Synthetic Aperture Radar (ALOS-PALSAR), the Envisat Advanced Synthetic Aperture Radar (ASAR), and the successor to Envisat ASAR, the Sentinel-1 SAR, which is operated by the European Space Agency (ESA).
- Since its presence in 2014, Sentinel-1 has attracted the attention of practitioners and researchers of radar remote sensing. Given that Sentinel-1 has a fairly high spatial and temporal resolution, it is also freely available to the public.
- In addition, Sentinel-1 released to the public has dual polarization, namely VV and VH. With high spatial and temporal resolution, as well as the availability of free and real time data, this makes Sentinel-1 SAR very feasible to be used in monitoring vegetation biophysical information.



Introduction (2)

- Despite the fact that SAR imagery such as Sentinel-1 has advantages over optical imageries in terms of minimizing atmospheric effects, it has one major drawback, namely the presence of speckle effects.
- Speckle, appearing in Synthetic Aperture Radar (SAR) imageries as granular noise, is due to the interference of waves reflected from many elementary scatterers.
- The speckle appears in SAR imageries due to the phenomenon of backscattering complexity of objects on the earth's surface.
- Speckle in SAR imageries complicates the imagery interpretation problem by reducing the effectiveness of image segmentation and classification.
- Notwithstanding the fact that the optical imageries have problems with atmospheric particles. The speckle effects in SAR imageries become kind of a distinct advantage for multispectral optical images such as Sentinel-2, because the optical imageries do not have the presence of speckle effects.
- So far, there are many speckle filtering methods that have been developed to reduce the speckle effect on radar imageries. Such as Lee, Lee Sigma, Refined Lee, Boxcar, Frost, Gamma Map, and Intensity-Driven Adaptive-Neighborhood (IDAN).
- Each speckle filtering method has different effects and capabilities. Even the same speckle filtering method can also be modified some parameters, for example the window processing size.
- Taking into account the advantages provided by SAR imageries such as Sentinel-1 in providing continuity of vegetation biophysical information, while SAR imageries themselves have problems with speckle effects. Of course, it is very necessary to test the ability of each speckle filtering method in reducing the speckle effect on SAR imageries. Especially when the SAR image will be used to extract vegetation biophysical information.

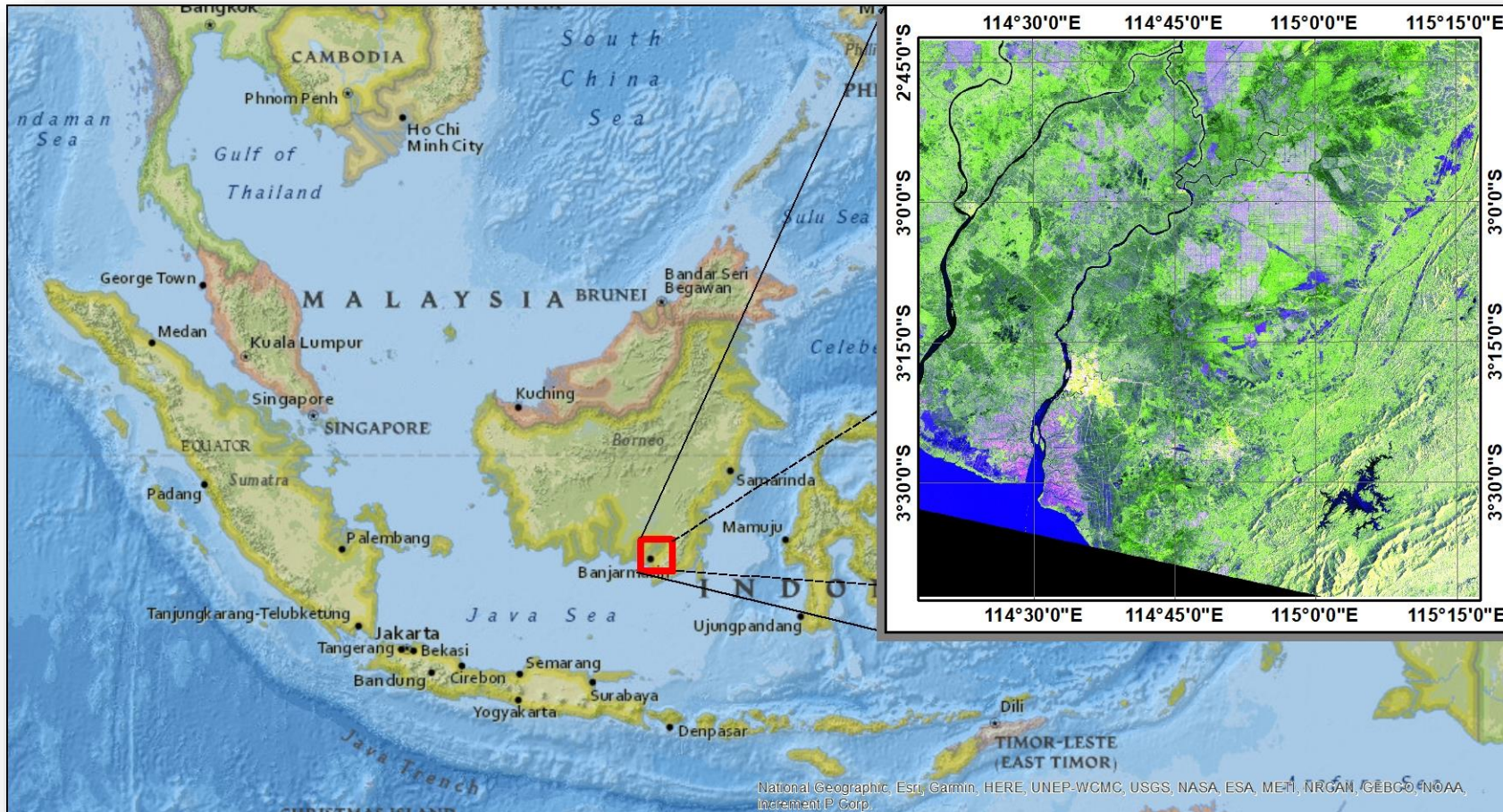


Research Purpose

The aim of this research is to test the ability of a number of speckle filtering methods to extract vegetation biophysical information from Sentinel-1 SAR.

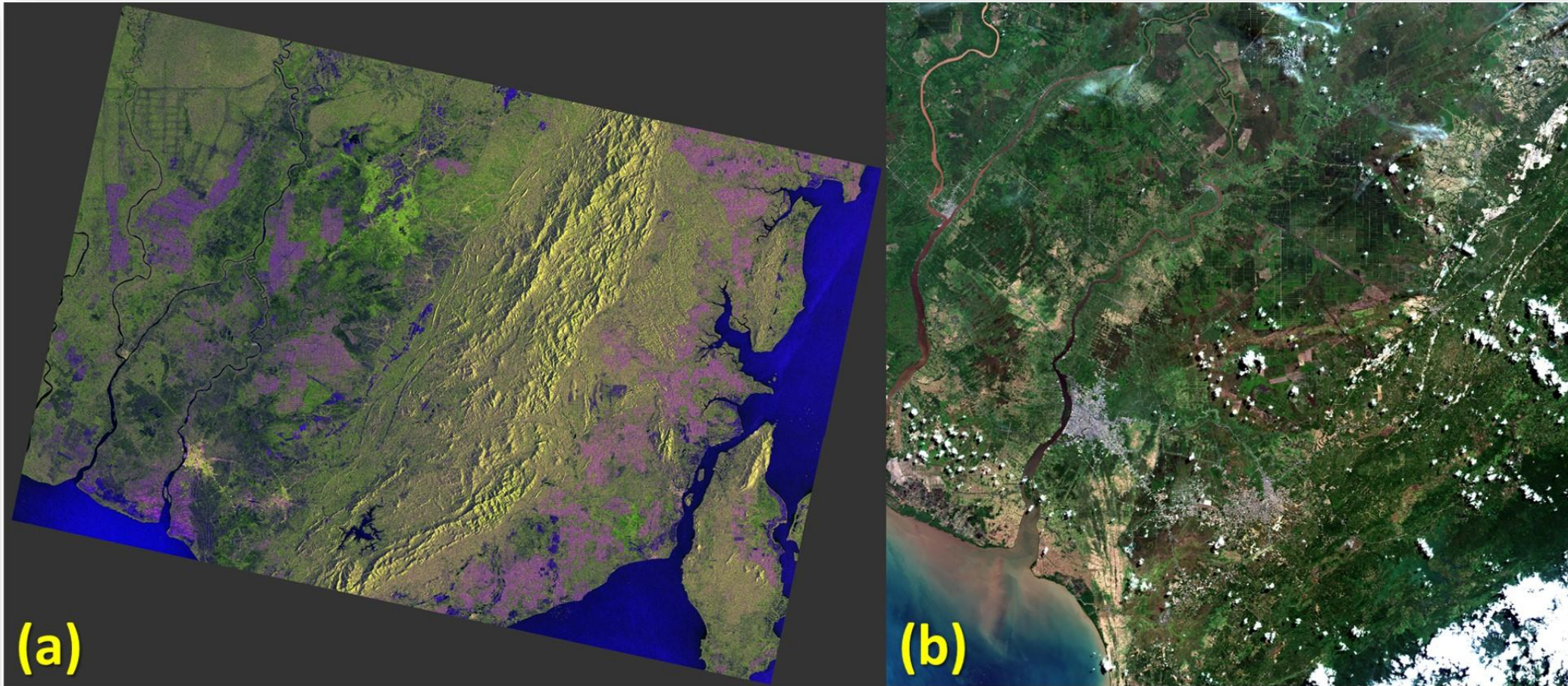
The expected significance of the results of this research is to obtain practical information about the most optimal speckle filtering techniques and parameters, in order to extract vegetation biophysical information from Sentinel-1 SAR imagery.

Research Location



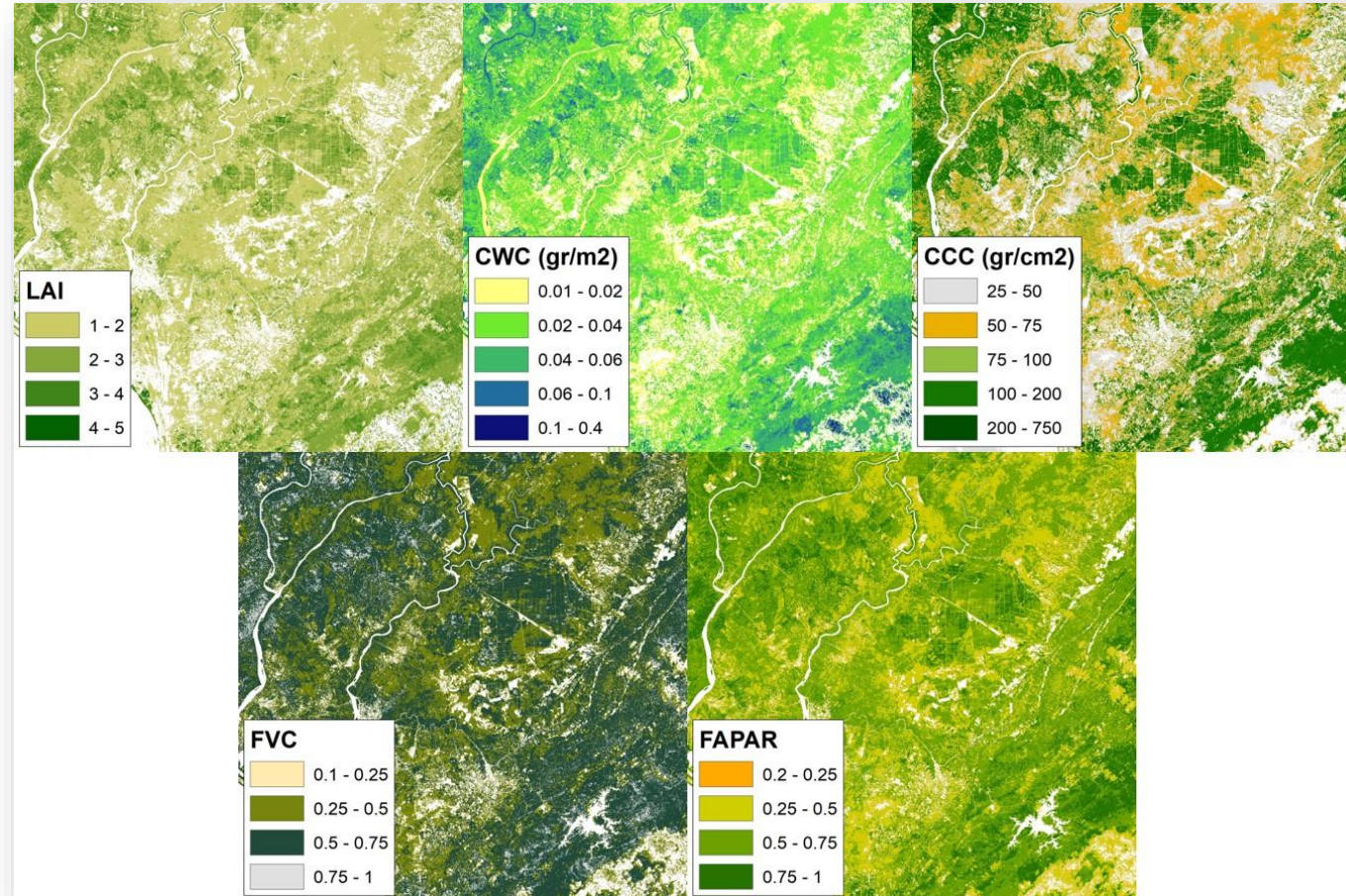
The research location is in the southern part of Kalimantan Island, Indonesia

Satellite Imageries



(a) Sentinel-1 SAR IW swath GRD and (b) Sentinel-2 MSI level 2A tile 50MKB were used in this research
(Acquired on July 30, 2019)

Vegetation Biophysical Information



Vegetation biophysical information extracted from Sentinel-2 MSI imagery

Image Pre-Processing and Speckle Filters

- The dual-polarized (VV, VH) Sentinel-1 SAR imagery calibrated into normalized Radar Cross Section (RCS), Sigma Nought (σ^0), using Sentinel-1 Toolbox (S1TBX) in SNAP application.
- The imagery is then multilooked and co-registered using SRTM 1-arc second, so that the spatial resolution becomes 10 meters.
- The level 2A pre-orthorectified Sentinel-2 MSI imagery is resampled using Sentinel-2 Toolbox (S2TBX) in SNAP application, so that all bands have a spatial resolution of 10 meters.
- Furthermore, for analysis purposes, the Sentinel-1 swath is then crop to adjust it to the Sentinel-2 tile 50MKB area boundary.
- Speckle filters are implemented on the calibrated and cropped Sentinel-1 imagery.
- There are several speckle filters to test, all of which are already available in the SNAP application tools. The speckle filters tested were Lee, Lee Sigma, Refined Lee, Frost, Gamma Map, Median, and IDAN.
- Several parameters in each speckle filtering method were modified, i.e. processing window sizes. The processing window sizes are set to vary, from 3x3 to 21x21. This applies to all speckle filtering methods, except Refined Lee and IDAN, which keep the default settings.
- Specifically for Lee Sigma, there are two variable parameter settings, namely processing window sizes and target window sizes. For Lee Sigma, the processing window sizes are set from 5x5 to 17x17, because the setting modes available in the SNAP application are indeed limited to those sizes. Meanwhile, for Lee Sigma's target window sizes, there are only two setting options, namely 3x3 and 5x5.



Dual Polarization SAR Vegetation Index (DPSVI)

The Dual Polarization SAR Vegetation Index (DPSVI) was developed to extract vegetation biomass information. The DPSVI is designed for dual-polarized SAR imageries. DPSVI is implemented on each Sentinel-1 imagery which has been speckle filtered. DPSVI is formulated as follows:

$$\text{DPSVI} = \frac{\sigma_{\text{vh}(i)}^0 \left[\left(\sigma_{\text{vv}(\text{max})}^0 \sigma_{\text{vh}(i)}^0 - \sigma_{\text{vv}(i)}^0 \sigma_{\text{vh}(i)}^0 + \sigma_{\text{vh}(i)}^{02} \right) + \left(\sigma_{\text{vv}(\text{max})}^0 \sigma_{\text{vv}(i)}^0 - \sigma_{\text{vv}(i)}^{02} + \sigma_{\text{vh}(i)}^0 \sigma_{\text{vv}(i)}^0 \right) \right]}{\sqrt{2} * \sigma_{\text{vv}(i)}^0}$$

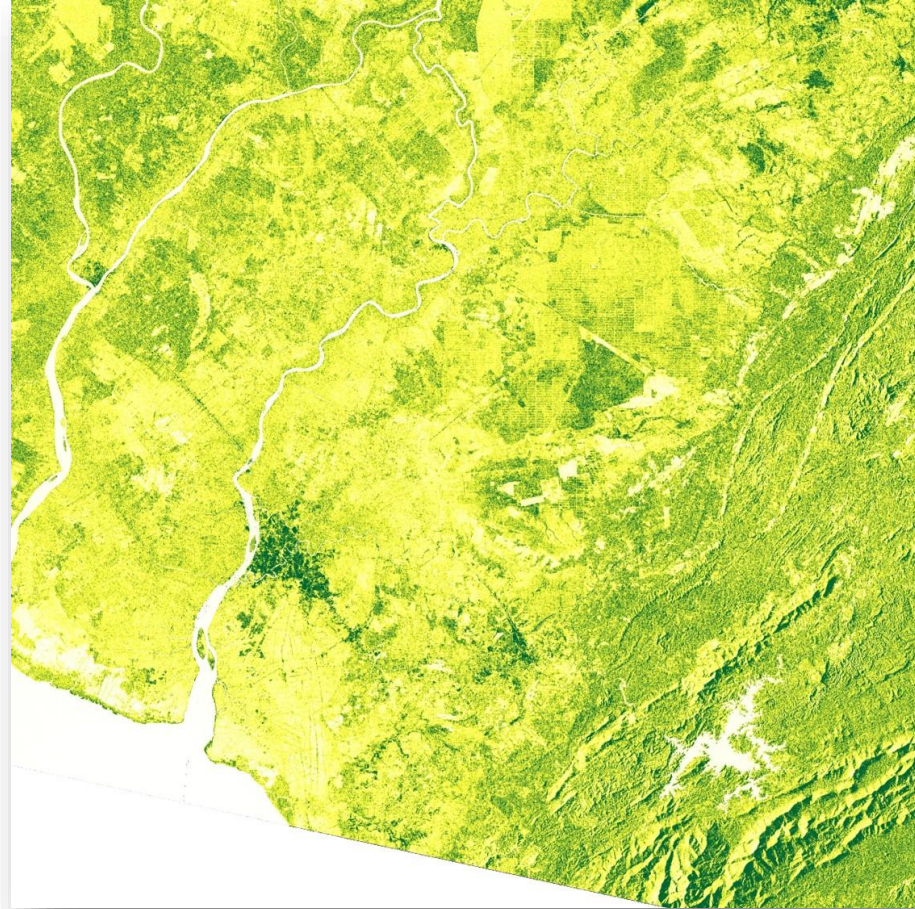
Where:

- σ_{VH}^0 : Sigma nought calibrated Sentinel-1 Vertical-Horizontal (VH) polarization
- σ_{VV}^0 : Sigma nought calibrated Sentinel-1 Vertical-Vertical (VV) polarization
- $\sigma_{\text{VV}(\text{max})}^0$: Maximum value of sigma nought calibrated Sentinel-1 Vertical-Vertical (VV) polarization

Just like the Normalized Difference Vegetation Index (NDVI) in optical imagery, DPSVI in dual-pol SAR is proportional to vegetation biophysical information. For example, the higher the DPSVI value, the higher the vegetation biomass will be, and vice versa. DPSVI is accurate enough to extract vegetation biophysical information from dual-polarized C-band SAR imageries such as Sentinel-1. Therefore, in this research, DPSVI is used as a parameter to test the ability of each speckle filtering method on Sentinel-1 imagery to extract vegetation biophysical information.



The DPSVI Image



DPSVI image using IDAN speckle filtering

Accuracy Assessment

The accuracy assessment is carried out using the Pearson Correlation Coefficient (PCC) (r), which is formulated as follows:

$$r = \frac{\sum_{i=1}^n (x_i - \bar{x})(y_i - \bar{y})}{\sqrt{\sum_{i=1}^n (x_i - \bar{x})^2} \sqrt{\sum_{i=1}^n (y_i - \bar{y})^2}}$$

Where:

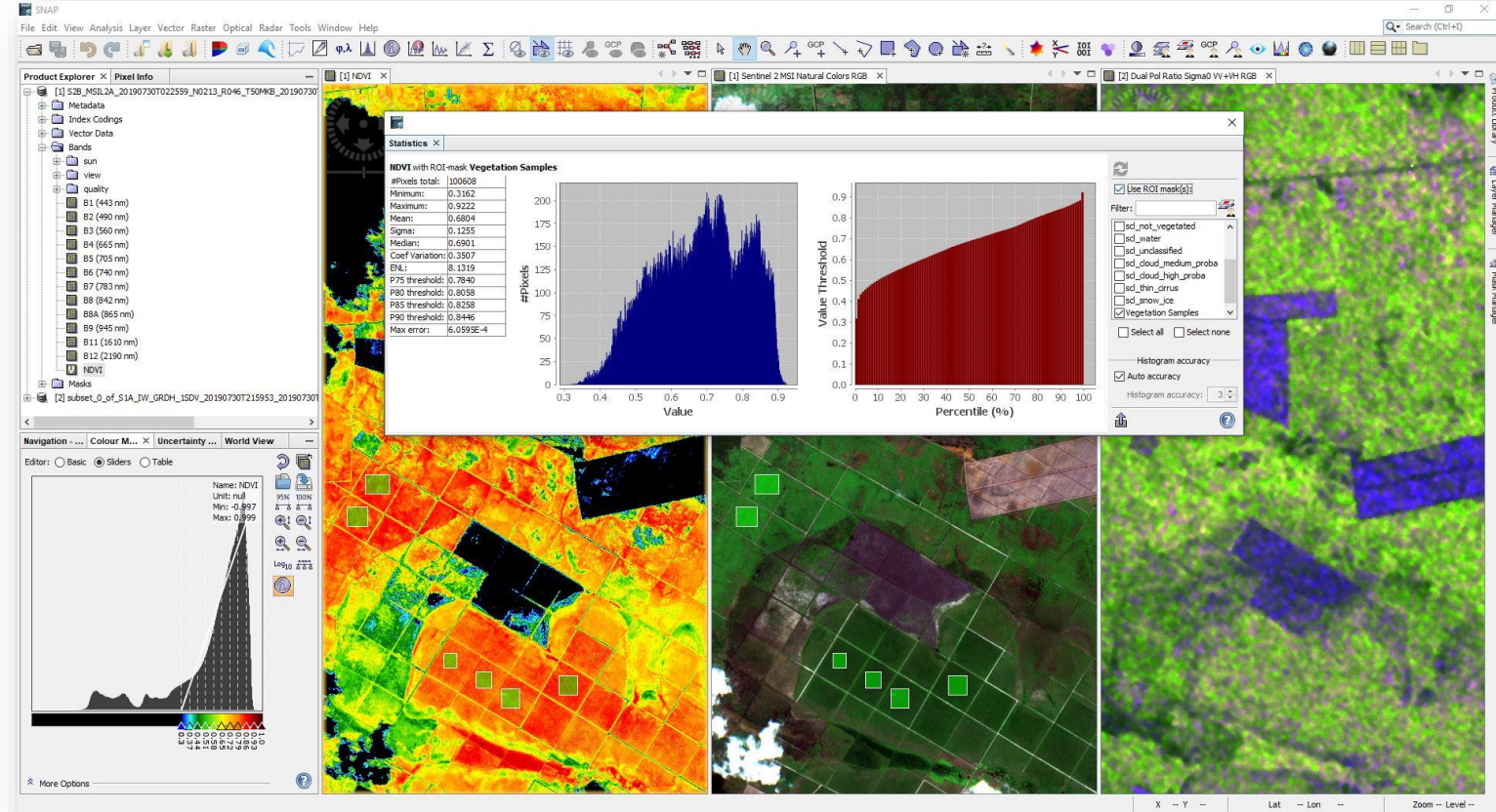
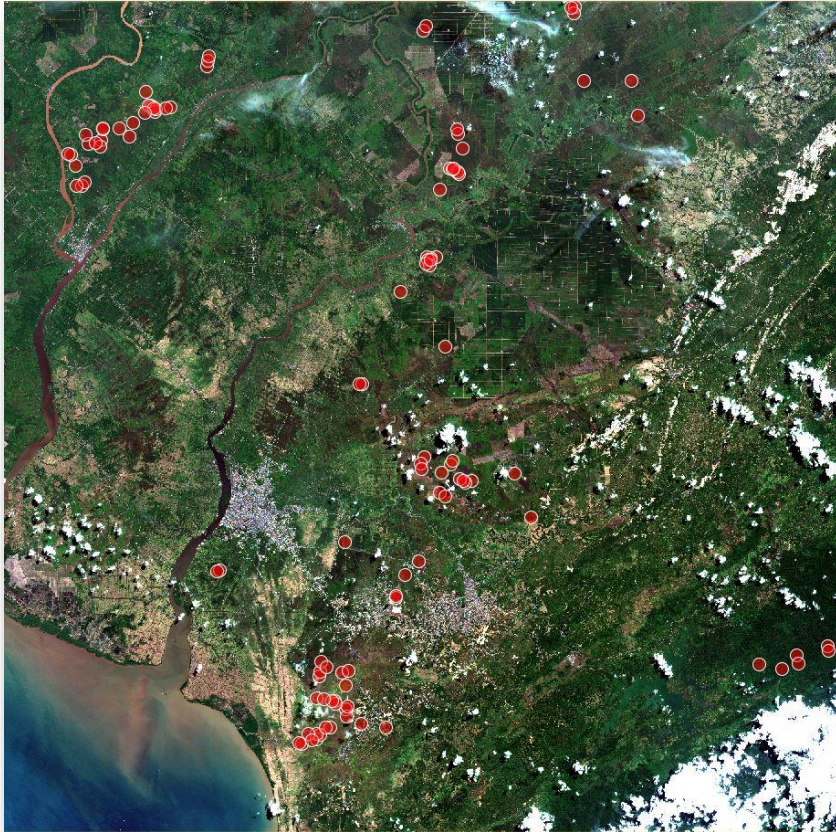
x_i : the i^{th} pixel of Sentinel-1 DPSVI

y_i : the i^{th} pixel of Sentinel-2 vegetation biophysical information

n : number of sample pixels

In the calculation of PCC (r), a sample of a number of pixels is required. The distribution and designation of sample pixels is carried out with the help of the NDVI transformation of Sentinel-2 imagery. This is because NDVI has been shown to have a fairly strong correlation with vegetation biophysical information. The distribution of sample pixels was carried out by stratified purposive sampling.

Sampling



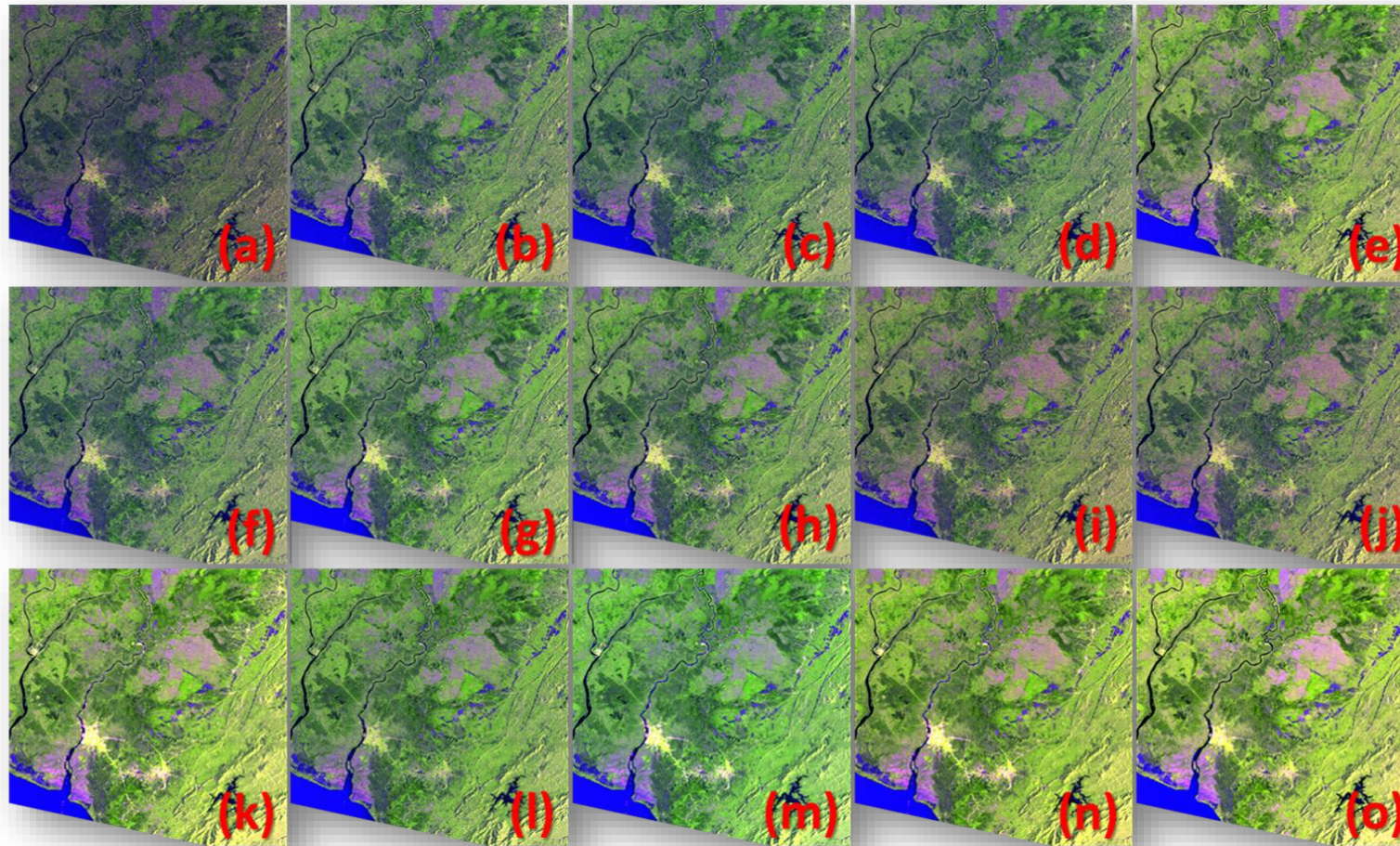
(Left) Distribution of sample locations on Sentinel-2 MSI true color composite imagery. There are a total of more than 100,000 pixels set as samples. (Right) In the designation of sample pixels, the statistical distribution of NDVI values is of great concern. The distribution of pixel values of the NDVI sample is attempted to approach the normal distribution, although it cannot be completely normal.

Window Size Simulation

- The target to be achieved in the search for the most optimal speckle filtering methods is to find a PCC value that reaches 0.8. Or in other words, the results of speckle filtering with vegetation biophysical information have a very strong correlation.
- If there is no PCC value that reaches 0.8 up to a processing window size of 21x21, then a simulation will be carried out to find the most optimal processing window size, so that later a PCC value of 0.8 can be obtained.
- The simulation of the processing window size was carried out using the regression method, based on the data of known PCC values up to the processing window size of 21x21. In this case, a scoring method is used on the processing window sizes. Namely, size 3x3 will be given a score of 3, size 5x5 will be given a score of 5, and so on, until size 21x21 will be given a score of 21.
- In the construction process of processing window size regression models, PCC values will be assigned as independent variables (x-axis). Meanwhile the processing window sizes will be placed as the dependent variable (y axis). The regression models applied are linear, exponential, logarithmic, power, and polynomial (quadratic).
- The regression equation which later has the highest correlation coefficient (r^2) is considered the best model to predict the most optimal processing window size in speckle filtering.



Result (1)



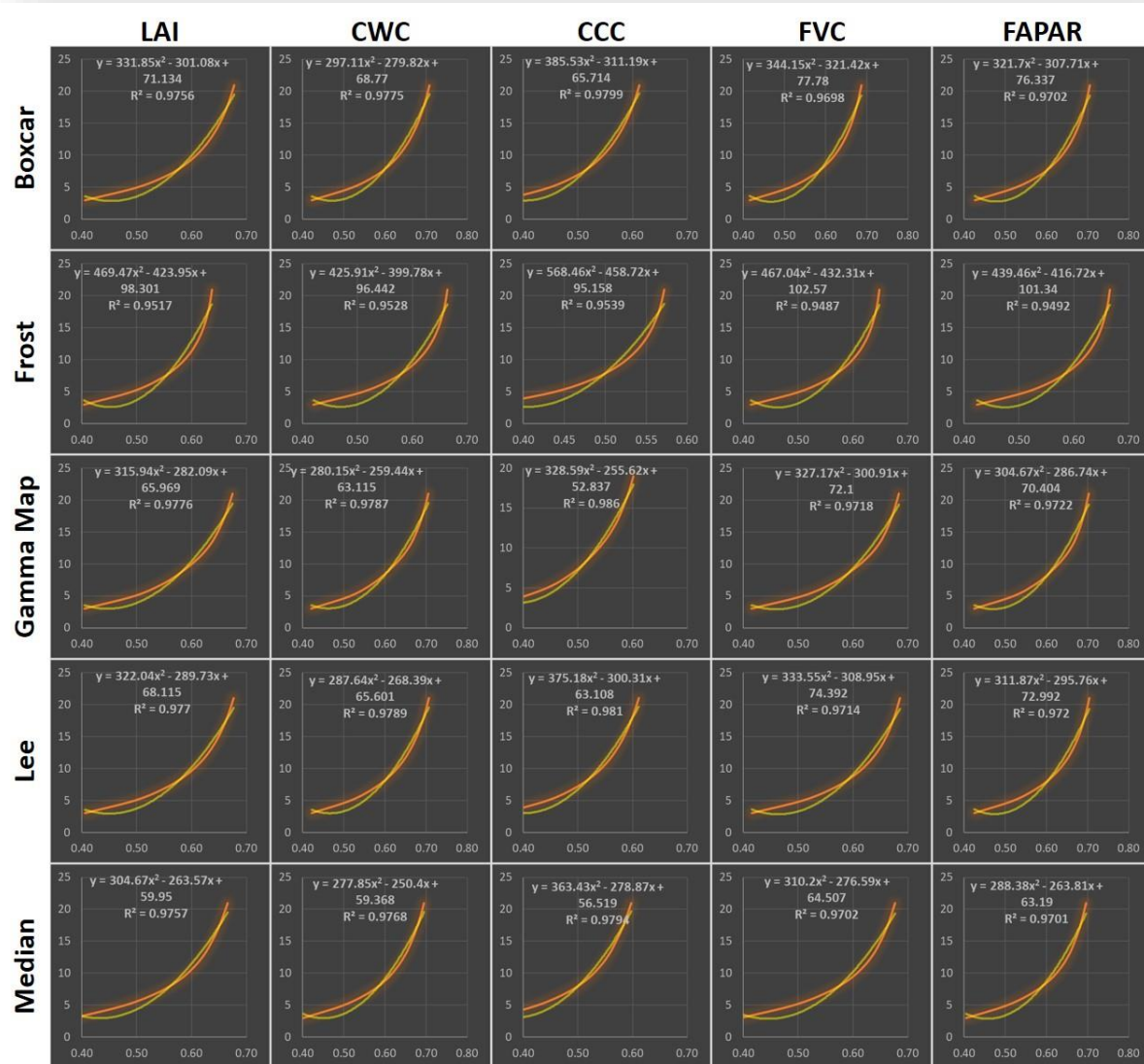
Unfiltered Sentinel-1 imagery and speckle filtered Sentinel-1 imageries. (a) Original imagery (unfiltered); (b) Boxcar 3x3; (c) Frost 3x3; (d) Gamma Map 3x3; (e) IDAN; (f) Lee 3x3; (g) Lee Sigma 7x7 (target window 3x3); (h) Lee Sigma 7x7 (target window 5x5); (i) Median 3x3; (j) Refined Lee; (k) Boxcar 37x37; (l) Frost 49x49; (m) Gamma Map 37x37; (n) Lee 37x37; and (o) Median 37x37.

Result (2)

| Speckle Filters | Parameters | Parameter Scoring | LAI | CWC | CCC | FVC | FAPAR |
|-------------------------------------|------------|-------------------|----------|----------|----------|----------|----------|
| Unfiltered | - | - | 0.296052 | 0.308913 | 0.263586 | 0.303591 | 0.311245 |
| Refined Lee | Default | - | 0.402843 | 0.419640 | 0.359107 | 0.413021 | 0.423679 |
| IDAN | Default | - | 0.560491 | 0.583778 | 0.500419 | 0.574348 | 0.589653 |
| Boxcar | 3x3* | 3 | 0.406172 | 0.422591 | 0.362794 | 0.416114 | 0.426334 |
| | 21x21 | 21 | 0.677627 | 0.707795 | 0.611872 | 0.686452 | 0.705157 |
| Frost | 3x3* | 3 | 0.403614 | 0.419940 | 0.360471 | 0.413520 | 0.423675 |
| | 21x21 | 21 | 0.636597 | 0.663570 | 0.571904 | 0.648247 | 0.665272 |
| Gamma Map | 3x3* | 3 | 0.405113 | 0.421601 | 0.361773 | 0.415049 | 0.425135 |
| | 21x21 | 21 | 0.674986 | 0.705630 | 0.609010 | 0.683636 | 0.702355 |
| Lee | 3x3* | 3 | 0.405462 | 0.421876 | 0.362130 | 0.415402 | 0.425554 |
| | 21x21 | 21 | 0.676754 | 0.706738 | 0.611098 | 0.685412 | 0.704030 |
| Median | 3x3* | 3 | 0.385276 | 0.401832 | 0.343492 | 0.394951 | 0.404840 |
| | 21x21 | 21 | 0.666001 | 0.695224 | 0.597863 | 0.676586 | 0.696588 |
| Lee Sigma (Target Window Size 3x3*) | 5x5 | 5 | 0.458273 | 0.478633 | 0.410470 | 0.467116 | 0.477632 |
| | 7x7* | 7 | 0.492558 | 0.515541 | 0.441533 | 0.501112 | 0.512294 |
| | 9x9 | 9 | 0.511214 | 0.535856 | 0.458516 | 0.519460 | 0.531077 |
| | 11x11 | 11 | 0.522779 | 0.548637 | 0.469182 | 0.530513 | 0.542501 |
| | 13x13 | 13 | 0.530884 | 0.557580 | 0.476849 | 0.537972 | 0.550220 |
| | 15x15 | 15 | 0.537240 | 0.564687 | 0.483119 | 0.543532 | 0.556024 |
| | 17x17 | 17 | 0.542143 | 0.570082 | 0.488110 | 0.548082 | 0.560726 |
| Lee Sigma (Target Window Size 5x5) | 5x5 | 5 | 0.447942 | 0.468408 | 0.401217 | 0.455599 | 0.465458 |
| | 7x7* | 7 | 0.479107 | 0.502305 | 0.429655 | 0.485929 | 0.496351 |
| | 9x9 | 9 | 0.495054 | 0.520080 | 0.444272 | 0.501220 | 0.512074 |
| | 11x11 | 11 | 0.505303 | 0.531432 | 0.453770 | 0.510875 | 0.521946 |
| | 13x13 | 13 | 0.512040 | 0.539001 | 0.460174 | 0.516981 | 0.528226 |
| | 15x15 | 15 | 0.516941 | 0.544539 | 0.465053 | 0.521155 | 0.532538 |
| | 17x17 | 17 | 0.520409 | 0.548459 | 0.468659 | 0.524069 | 0.535504 |



Result (3)



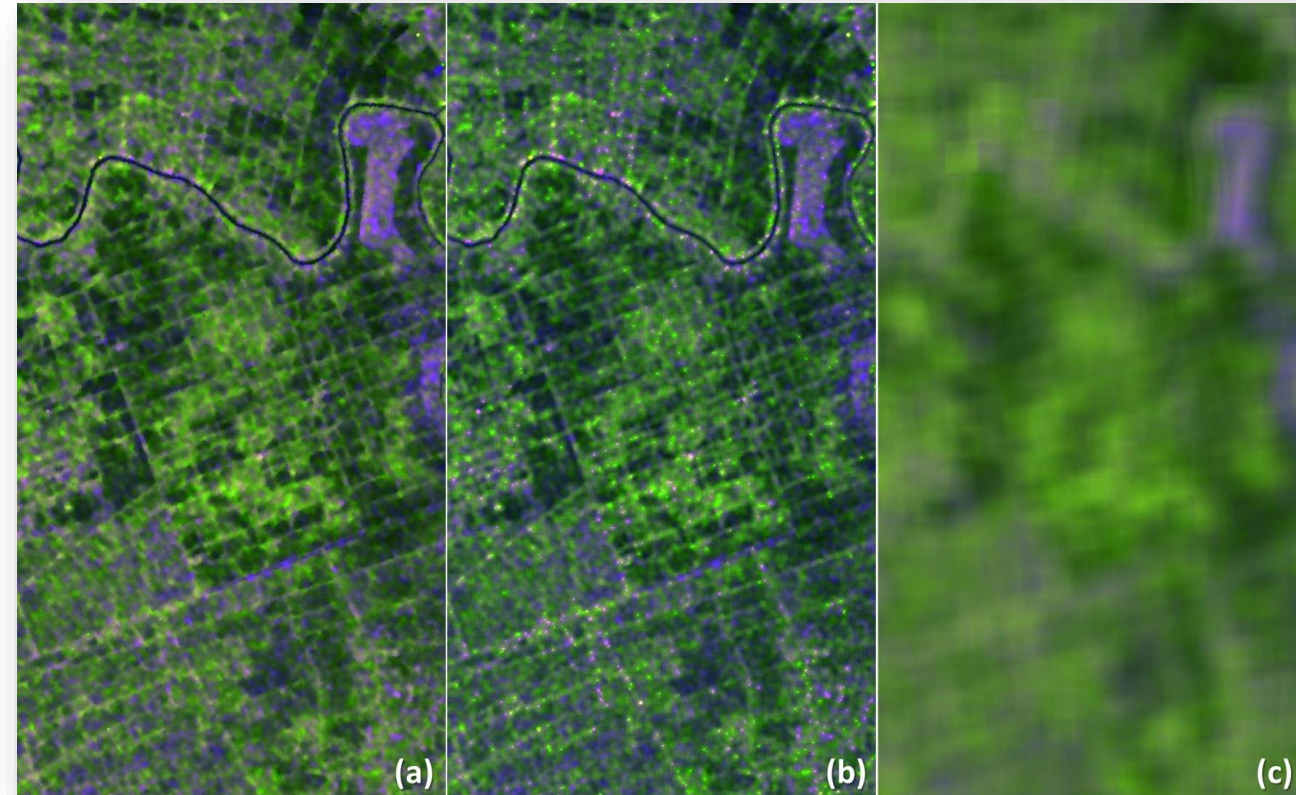
- The entire speckle filtering method for each vegetation biophysical information parameter shows a polynomial (quadratic) correlation with increasing processing window sizes.
- In Fig., we only present the test regression models with the highest correlation coefficients (r^2). Because it would be too much if we had to display graphs for all the regression models tested in this study.
- Overall r^2 shows a value of 0.9 more, this means between the increase in processing window sizes with accuracy (r). However, since the correlations are quadratic, it could be predicted that at some point the values of r will be saturated, even though the processing window sizes in speckle filtering are enlarged.
- In other words, increasing the processing window sizes to certain sizes will no longer be able to significantly increase the accuracy of the speckle filtering methods.

Result (4)

Estimated processing window sizes for each method of speckle filtering and vegetation biophysical information to reach a PCC value of 0.8

| | LAI | CWC | CCC | FVC | FAPAR |
|-----------|---------|---------|---------|---------|---------|
| Boxcar | 43 x 43 | 35 x 35 | 65 x 65 | 41 x 41 | 37 x 37 |
| Frost | 61 x 61 | 49 x 49 | 93 x 93 | 57 x 57 | 49 x 49 |
| Gamma Map | 43 x 43 | 35 x 35 | 59 x 59 | 41 x 41 | 37 x 37 |
| Lee | 43 x 43 | 35 x 35 | 63 x 63 | 41 x 41 | 37 x 37 |
| Median | 45 x 45 | 37 x 37 | 67 x 67 | 43 x 43 | 37 x 37 |

The results of the speckle filtering using the simulated window sizes were then retested using PCC. The test results show that the highest r value for Boxcar is 0.735194, for Frost is 0.668937, for Gamma Map is 0.730305, for Lee is 0.733073, and for Median is 0.730752.



Visual comparison between (a) IDAN, (b) Lee Sigma 7x7 (target window size 3x3), and (c) Boxcar 37x37

Conclusions

1. In this research, we focus more on presenting a comparison of the capabilities of several speckle filtering methods to extract various vegetation biophysical information parameters. Without having to review further the fundamental concepts of each speckle filtering method.
2. The results of the research show that in setting the default parameters using SNAP software, IDAN and Lee Sigma are able to provide the best performance. However, these two filters are less flexible in setting processing window sizes.
3. When the processing window sizes are set to 21x21, the Boxcar method and Lee's method give the best results, with the PCC values ranging from 0.6s to 0.7s. Even when processing window sizes are simulated to reach a PCC value of 0.8, Boxcar still delivers the best output.
4. Despite the fact that the PCC value of 0.8 was never achieved in this research, this was due to the limited number of samples in the simulation. Of course, with the consequence of decreasing the spatial resolution of the image and losing certain details on the image.



Acknowledgements

This research was funded by the Center for Geospatial Information Infrastructure Development (PPIIG) of Universitas Lambung Mangkurat, Banjarbaru, Indonesia. We thank the European Space Agency (ESA) which has provided Sentinel-1 SAR imagery, Sentinel-2 MSI imagery, and SNAP software for free. And also to the Geospatial Information Laboratory, Faculty of Forestry, Universitas Lambung Mangkurat, which has facilitated digital imagery processing in this research.



Transfer Of Copyright To Society Of Photo-Optical Instrumentation Engineers (SPIE)

SPIE Paper No. GSS21-5
Title of Paper On finding optimal speckle filtering for extraction of vegetation biophysical information using Sentinel-1 SAR imagery
Author(s) Ali, Syamani D., University of Lambung Mangkurat; Fithria, Abdi, University of Lambung Mangkurat; Rahmadi, Adi; Rezekiah, Arfa A.;
Contact Author Email syamani.fhut@ulm.ac.id

This Agreement must be signed and returned to SPIE prior to publication of the Paper referenced above in an SPIE Conference Proceedings or Journal. The intent of this Agreement is to protect the interests of both SPIE and authors/employers and to specify reasonable rights for both parties related to publication and reuse of the material.

The undersigned hereby assigns to Society of PhotoOptical Instrumentation Engineers (SPIE) copyright ownership in the above Paper, effective if and when the Paper is accepted for publication by SPIE and to the extent transferable under applicable national law. This assignment gives SPIE the right to register copyright to the Paper in its name as claimant and to publish the Paper in any print or electronic medium.

Authors, or their employers in the case of works made for hire, retain the following rights:

1. All proprietary rights other than copyright, including patent rights.
2. The right to make and distribute copies of the Paper for internal purposes.
3. The right to use the material for lecture or classroom purposes.
4. The right to prepare derivative publications based on the Paper, including books or book chapters, journal papers, and magazine articles, provided that publication of a derivative work occurs subsequent to the official date of publication by SPIE.
5. The right to post an author-prepared version or an official version (preferred version) of the published paper on an internal or external server controlled exclusively by the author/employer, provided that (a) such posting is noncommercial in nature and the paper is made available to users without charge and (b) a copyright notice and full citation appear with the paper, including the DOI.

Citation format:

Author(s), "Paper Title", Publication Title, Editors, Volume (Issue) Number, Article (or Page) Number, (Year); DOI.

Copyright notice format:

Copyright XXXX (year) Society of PhotoOptical Instrumentation Engineers. One print or electronic copy may be made for personal use only. Systematic reproduction and distribution, duplication of any material in this paper for a fee or for commercial purposes, or modification of the content of the paper are prohibited.

If the work that forms the basis of this Paper was done under a contract with a governmental agency or other entity that retains certain rights, this Transfer of Copyright is subject to any rights that such governmental agency or other entity may have acquired.

By signing this Agreement, the authors warrant that (1) the Paper is original and has not previously been published elsewhere; (2) the Paper does not infringe on any copyright or other rights in any other work; (3) all necessary reproduction permissions, licenses, and clearances have been obtained; and (4) the authors own the copyright in the Paper, are authorized to transfer it, and have full power to enter into this Agreement with SPIE.

WHO SHOULD SIGN?

Were ALL authors on this paper employees of the U.S. Government when this paper was prepared and was this paper prepared as part of their official duties?

Copyright Signature:

Syamani D. Ali
On finding optimal speckle filtering for extr:
9 September 2021

Copyrights, SPIE, P.O. Box 10, Bellingham, WA 98227-0010 USA
Phone: 360-676-3290 (Pacific Time) • Fax: 360-647-1445 • copyrights@spie.org

Revised 1 January 2017

On Finding Optimal Speckle Filtering for Extraction of Vegetation Biophysical Information Using Sentinel-1 SAR Imagery

Syamani D. Ali^{*a}, Abdi Fithria^a, Adi Rahmadi^a, Arfa A. Rezekiah^a

^aFaculty of Forestry, University of Lambung Mangkurat, Jl. Ahmad Yani km. 35, Banjarbaru, 70714, South Kalimantan, Indonesia

^aCenter for Geospatial Information Infrastructure Development (PPIIG), University of Lambung Mangkurat, Jl. Ahmad Yani km. 35, Banjarbaru, 70714, South Kalimantan, Indonesia

ABSTRACT

The SAR imagery such as Sentinel-1 in general has a major problem with the speckle effects. There are many speckle filtering methods have been developed to reduce the speckle effect. This research aims to test the ability of a number of speckle filtering methods to extract vegetation biophysical information from Sentinel-1. The ground truth of vegetation biophysical information in this research were simulated using Sentinel-2 MSI imagery. That is, Leaf Area Index (LAI), Canopy Water Content (CWC), Canopy Chlorophyll Content (CCC), Fraction of Vegetation Cover (FVC), and Fraction of Absorbed Photosynthetically Active Radiation (FAPAR). The Sentinel-1 imagery was speckle filtered using various methods, namely Lee, Lee Sigma, Refined Lee, IDAN, Boxcar, Frost, Gamma Map, and Median. Some speckle filtering parameters were modified, i.e. the processing windows. The Dual Polarization SAR Vegetation Index (DPSVI) were then extracted from the speckle-filtered Sentinel-1. DPSVI were then tested for correlation with vegetation biophysical information using the Pearson Correlation Coefficient (r). The test results show that Boxcar produces the highest r values for all types of vegetation biophysical information, with values ranging from 0.6s to 0.7s. Followed by Lee, Gamma Map, Median, and Frost. Each with a processing window size of 21x21. Since there are no r values was found which reached 0.8 for processing window sizes up to 21x21, the simulation was then run using the regression method. The simulation results show that to achieve r values of 0.8, it is predicted that window sizes range from 35x35 to 93x93.

Keywords: Speckle filtering, Synthetic Aperture Radar, Sentinel-1, Sentinel-2, vegetation biophysics, correlation

*syamani.fhut@ulm.ac.id; phone 62 511 330-6694; fax 62 511 330-6694; ulm.ac.id

1. INTRODUCTION

The ability of multispectral optical imageries such as Landsat series, Sentinel-2 MSI, Sentinel-3 OLCI, or others, in extracting vegetation biophysical information above the earth's surface is unquestionable. Various research results have proven this. Ref. 9 validated the Sentinel Simplified Level 2 Product Prototype Processor (SL2P) for mapping cropland biophysical variables using Sentinel-2 MSI and Landsat-8 OLI data. They found that SL2P presents good performances to estimate Leaf Area Index (LAI) and Fraction of Vegetation Cover (FVC) from both MSI and OLI data. Ref. 31 conducted a mapping and monitoring of woody vegetation canopy cover and height at a regional scale using Landsat time-series data, from 2000 to 2017. They found that tree height estimates had a correlation coefficient of 0.92 and the r^2 of 0.85. Ref. 16 estimates LAI for Landsat imageries over the contiguous United States. They found that LAI estimates show an overall Root Mean Squared Error (RMSE) of 0.8 with r^2 of 0.88. Ref. 44 used the Sentinel-3 Ocean and Land Color Instrument (OLCI) to derive LAI information. Field measurements of LAI at two forest sites quantitatively confirm that the estimated LAI from OLCI is reasonably accurate with $r^2 > 0.65$ and $RMSE < 1.00 \text{ m}^2\text{m}^{-2}$ 44. Ref. 8 validated the extracted LAI information using Sentinel-2 Level 2 Prototype Processor (SL2P) and modified version of Sentinel-2 Level 2 Prototype Processor (SL2P-D). The results showed that both of them demonstrated good performance, with SL2P-D slightly more accurate than SL2P.

In fact, there are countless research that prove the power of optical imageries in extracting vegetation biophysical information. However, optical imageries such as Sentinel-2 MSI have a major drawback, which is that they are very sensitive to atmospheric disturbances. For tropical areas such as Indonesia, which always experience the presence of atmospheric disturbances such as clouds, monitoring the vegetation biophysical information throughout time continuously is a special challenge. Ref. 13 stated that a dense time series of optical satellite imagery describing vegetation activity

provides essential information for the efficient and regular monitoring of vegetation. Nevertheless, the temporal resolution of optical sensors is strongly affected by cloud cover, resulting in significant missing information¹³. The use of complementary acquisitions, such as Synthetic Aperture Radar (SAR) data, opens the door to the development of new multi-sensor methodologies aiming at the reconstruction of missing information¹³.

Recently, there are many SAR imaging technologies that have been developed, which can be used to extract vegetation biophysical information. Such as the Advanced Land Observing Satellite-Phased Array L-band Synthetic Aperture Radar (ALOS-PALSAR), the Envisat Advanced Synthetic Aperture Radar (ASAR), and the successor to Envisat ASAR, the Sentinel-1 SAR, which is operated by the European Space Agency (ESA). Since its presence in 2014, Sentinel-1 has attracted the attention of practitioners and researchers of radar remote sensing. Given that Sentinel-1 has a fairly high spatial and temporal resolution, it is also freely available to the public. In addition, Sentinel-1 released to the public has dual polarization, namely VV and VH. With high spatial and temporal resolution, as well as the availability of free and real time data, this makes Sentinel-1 SAR very feasible to be used in monitoring vegetation biophysical information.

Various research have been carried out to extract vegetation biophysical information from the Sentinel-1 SAR imagery. Ref. 30 developed the Dual Polarization SAR Vegetation Index (DPSVI) for biomass information retrieval using Sentinel-1. The results showed that between DPSVI and Above Ground Biomass (AGB) had r^2 values of 0.7 and above. Ref. 24 derives a new vegetation index from dual-pol SAR, namely the Dual-polarimetric Radar Vegetation Index (DpRVI). Their research results show that DpRVI has r^2 values ranging from 0.7s to 0.8s for certain vegetation biophysical parameters. There is one model that is often used as a method for extracting vegetation biophysical information from SAR imageries such as Sentinel-1, namely the Water Cloud Model (WCM)^{2,15}. There has been a considerable amount of research using WCM to extract vegetation biophysical information from Sentinel-1. For examples Ref. 3, 4, 5, 25, 43, and so on.

Despite the fact that SAR imagery such as Sentinel-1 has advantages over optical imageries in terms of minimizing atmospheric effects, it has one major drawback, namely the presence of speckle effects. Speckles are a direct result of the coherent incident energy, which can be assumed to have a single frequency and the wavefront arrives at a single-phase pixel³³. Speckle, appearing in Synthetic Aperture Radar (SAR) imageries as granular noise, is due to the interference of waves reflected from many elementary scatterers²². The speckle appears in SAR imageries due to the phenomenon of backscattering complexity of objects on the earth's surface³⁸. Speckle in SAR imageries complicates the imagery interpretation problem by reducing the effectiveness of image segmentation and classification²². This is a distinct advantage for multispectral optical images such as Sentinel-2, because it does not have the presence of a speckle effect. Even though the optical imageries have problems with atmospheric particles.

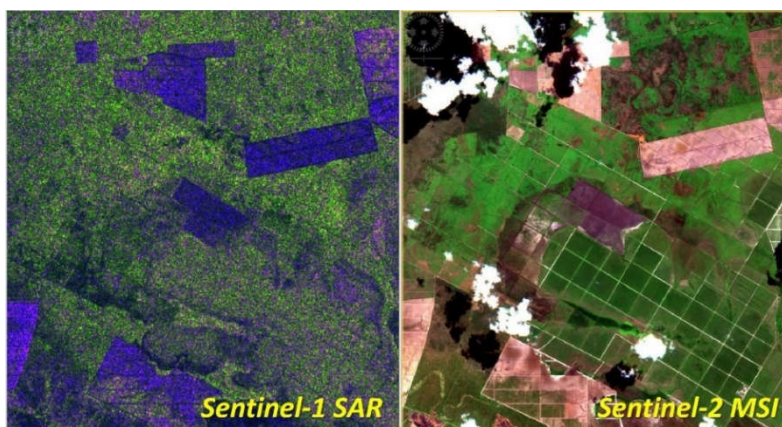


Fig. 1. Sentinel-1 and Sentinel-2 at the same location and acquisition date. SAR imagery is relatively clean from atmospheric disturbances, but is decorated by speckle effects. Optical imagery has no speckle effect but is susceptible to atmospheric disturbances.

So far, there are many speckle filtering methods that have been developed to reduce the speckle effect on radar imageries. Such as Lee¹⁹, Lee Sigma^{20,21}, Refined Lee⁴⁵, Boxcar²³, Frost¹², Gamma Map⁶, and Intensity-Driven Adaptive-Neighborhood (IDAN)⁴⁰. Each speckle filtering method has different effects and capabilities. Even the same speckle filtering method can also be modified some parameters, for example the window processing size. There are quite a number of previous studies that have tested the capabilities of each speckle filtering technique. As has been implemented by Ref. 1, 7, 10, 11, 14, 18, 26, 28, 32, 35, and 39.

Ref. 14 tested the performance of various speckle filtering methods on Sentinel-1, namely Frost, Gamma-MAP, Median, and Refined Lee, for modeling forest aboveground biomass (AGB). Their research results show that Frost provides the best correlation between AGB and backscatter. The value of r^2 is 0.3464158 and RMSE is 33.5231. Ref. 26 evaluated a number of speckle filtering methods for Polarimetric SAR (PolSAR) data. The filter methods tested were Boxcar, Lee Sigma, Refined Lee, Lopez, and IDAN. They found that IDAN was the best, because it had the smallest bias among all evaluated filter methods. However, they also found that the Boxcar was visually effective in reducing speckle. Although in the Boxcar filter results a lot of detail is lost due to blurring. Ref. 28 assessed a number of speckle filtering methods for the purposes of Object Based Image Analysis (OBIA). They found that the NL-SAR filter gave the best results. Ref. 30 uses the Refined Lee method to reduce noise on Sentinel-1, when testing the correlation between DPSVI and AGB. The results showed that the value of r^2 was in the range of 0.7s. Although in the research, Ref. 30 did not provide any argument for using Refined Lee.

Taking into account the advantages provided by SAR imageries such as Sentinel-1 in providing continuity of vegetation biophysical information, while SAR imageries themselves have problems with speckle effects. Of course, it is very necessary to test the ability of each speckle filtering method in reducing the speckle effect on SAR imageries. Especially when the SAR image will be used to extract vegetation biophysical information. The aim of this research is to test the ability of a number of speckle filtering methods to extract vegetation biophysical information from Sentinel-1 SAR. The expected significance of the results of this research is to obtain practical information about the most optimal speckle filtering techniques and parameters, in order to extract vegetation biophysical information from Sentinel-1 SAR imagery.

2. RESEARCH LOCATION AND DATA

2.1 Research Location

This research took samples of Sentinel-1 and Sentinel-2 in the southern part of Kalimantan or Borneo Island, Indonesia. This area covers the entire 50MKB Sentinel-2 MSI imagery tile area, with an area approximate to 110 kilometers x 110 kilometers. Administratively, most of this research area belongs to South Kalimantan Province, and a small part belongs to Central Kalimantan Province.

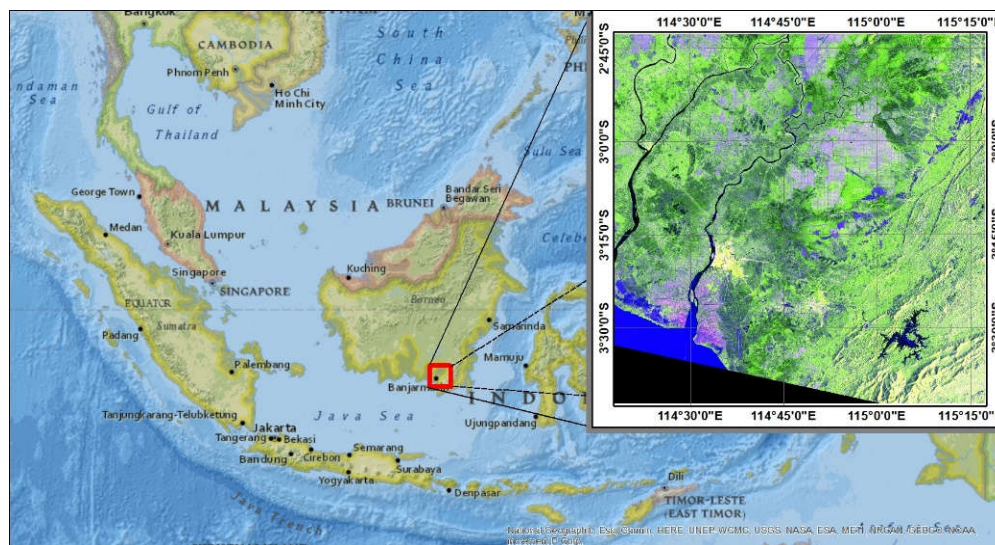


Fig. 2. The research location is in the southern part of Kalimantan Island, Indonesia

The main reason for choosing this research area is because the vegetation cover conditions in this area are very heterogeneous. Which consists of primary dryland forest, secondary dryland forest, swamp forest, peatland forest, mangrove forest, plantation forest, rubber plantation, oil palm plantation, mixed garden, fields/moorlands, rice fields, shrubs and bushes, swamp shrubs and bushes, and grasslands. The heterogeneity of vegetation features is very important in sampling for accuracy testing in this research. So that later the resulting accuracy can represent or at least approach the overall condition of the vegetation features.

2.2 Satellite Imageries

There are two satellite imageries used in this, namely Sentinel-1 Synthetic Aperture Radar (SAR) and Sentinel-2 Multispectral Instrument (MSI). Where both imageries are provided by the European Space Agency (ESA) free of charge. The selection process of the two imageries was done in such a way that the acquisition date of the two imageries is exactly the same. This is to ensure that there are no differences or changes in vegetation conditions in the two imageries. The Sentinel-1 SAR Interferometric Wide (IW) swath Ground Range Detected (GRD) product imagery used is S1A_IW_GRDH_1SDV_20190730T215953_20190730T220018_028352_03342D_4B6F, acquired on 30 July 2019, 21:59:53 GMT or 05:59:53 local time (Central Indonesia Time). The Sentinel-2 MSI imagery used is S2B_MSIL2A_20190730T022559_N0213_R046_T50MKB_20190730T062914, acquired on 30 July 2019, at 02:25:59 GMT or 10:25:59 local time. The Sentinel-2 (tile 50MKB) imagery used is Sentinel-2B level 2A Bottom of Atmospheric (BOA) reflectance and has been topographically corrected by ESA, considering that later vegetation biophysical information will be extracted quantitatively from Sentinel-2.

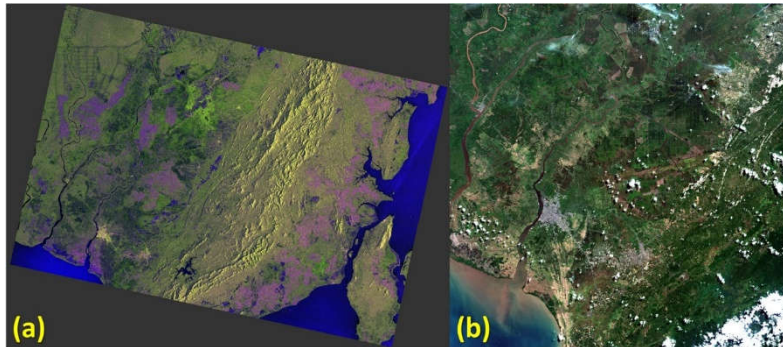


Fig. 3. (a) Sentinel-1 SAR IW swath GRD and (b) Sentinel-2 MSI level 2A tile 50MKB were used in this research.

2.3 Vegetation Biophysical Information

There are no ground surveys were conducted in this research. The ground truth of vegetation biophysical information in this research was simulated using vegetation biophysical information extracted quantitatively from MSI Sentinel-2 imagery. In this case, vegetation biophysical information was extracted automatically using the S2 SNAP Toolbox biophysical variable⁴², which is integrated in the Sentinel Application Platform (SNAP) software provided free of charge by the ESA. There are five vegetation biophysical information that would be extracted using this tool, namely Leaf Area Index (LAI), Canopy Water Content (CWC), Canopy Chlorophyll Content (CCC), Fraction of Vegetation Cover (FVC), and Fraction of Absorbed Photosynthetically Active Radiation (FAPAR).

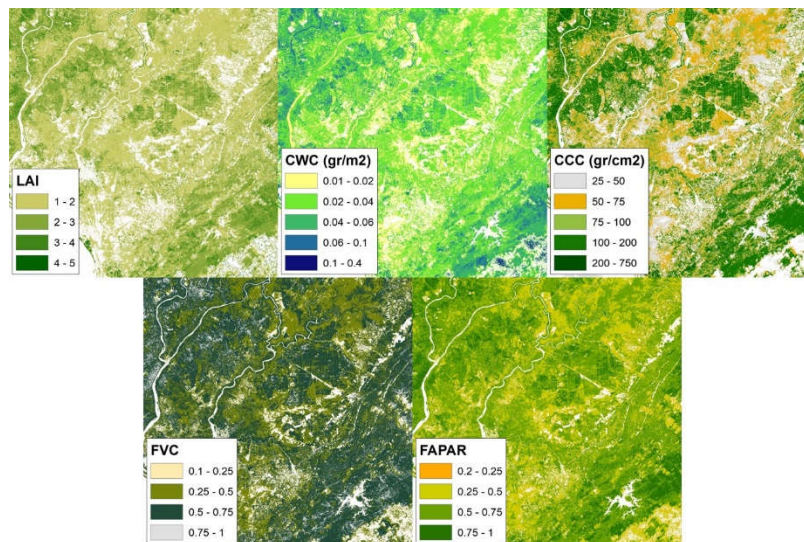


Fig. 4. Vegetation biophysical information extracted from Sentinel-2 MSI imagery.

It is certain that vegetation biophysical information from Sentinel-2 will not be as accurate as information directly from the field. However, this research will at least get an overview of the relative capabilities especially when compared to each other for each speckle filtering method in extracting vegetation biophysical information. When tested in the African semi-arid agricultural landscape, LAI products extracted from Sentinel-2 using SNAP application, were found to have r^2 of 0.6 to 0.7 with in-situ data. With a fairly large Mean Absolute Error (MAE), which is $> 2 \text{ m}^2\text{m}^{-2}$ ¹⁷.

3. RESEARCH METHODOLOGY

3.1 Image Pre-Processing

The dual-polarized (VV, VH) Sentinel-1 SAR imagery calibrated into normalized Radar Cross Section (RCS), Sigma Nought (σ^0), using Sentinel-1 Toolbox (S1TBX) in SNAP application. The imagery is then multilooked and co-registered using SRTM 1-arc second, so that the spatial resolution becomes 10 meters. The level 2A pre-orthorectified Sentinel-2 MSI imagery is resampled using Sentinel-2 Toolbox (S2TBX) in SNAP application, so that all bands have a spatial resolution of 10 meters. Furthermore, for analysis purposes, the Sentinel-1 swath is then crop to adjust it to the Sentinel-2 tile 50MKB area boundary.

3.2 Speckle Filters

Speckle filters are implemented on the calibrated and cropped Sentinel-1 imagery. There are several speckle filters to test, all of which are already available in the SNAP application tools. The speckle filters tested were Lee, Lee Sigma, Refined Lee, Frost, Gamma Map, Median, and IDAN. Several parameters in each speckle filtering method were modified, i.e. processing window sizes. The processing window sizes are set to vary, from 3x3 to 21x21. This applies to all speckle filtering methods, except Refined Lee and IDAN, which keep the default settings. Specifically for Lee Sigma, there are two variable parameter settings, namely processing window sizes and target window sizes. For Lee Sigma, the processing window sizes are set from 5x5 to 17x17, because the setting modes available in the SNAP application are indeed limited to those sizes. Meanwhile, for Lee Sigma's target window sizes, there are only two setting options, namely 3x3 and 5x5.

3.3 Dual Polarization SAR Vegetation Index (DPSVI)

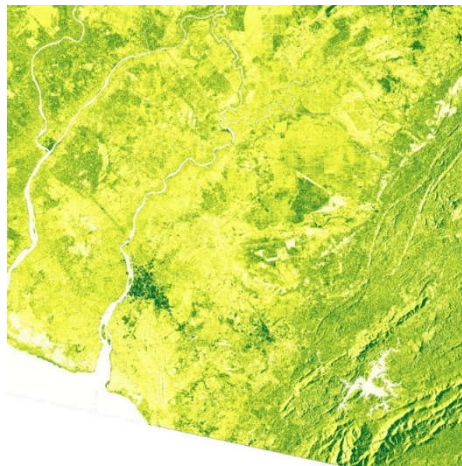


Fig. 5. DPSVI image using IDAN speckle filtering.

The Dual Polarization SAR Vegetation Index (DPSVI) was developed to extract vegetation biomass information³⁰. The DPSVI is designed for dual-polarized SAR imageries. DPSVI is implemented on each Sentinel-1 imagery which has been speckle filtered. DPSVI is formulated as follows³⁰:

$$DPSVI = \frac{\sigma_{vh(i)}^0 \left[\left(\sigma_{vv(max)}^0 \sigma_{vh(i)}^0 - \sigma_{vv(i)}^0 \sigma_{vh(i)}^0 + \sigma_{vh(i)}^0 \right) + \left(\sigma_{vv(max)}^0 \sigma_{vv(i)}^0 - \sigma_{vv(i)}^0 + \sigma_{vh(i)}^0 \sigma_{vv(i)}^0 \right) \right]}{\sqrt{2} * \sigma_{vv(i)}^0} \quad (1)$$

Where:

σ_{VH}^0 : Sigma nought calibrated Sentinel-1 Vertical-Horizontal (VH) polarization

σ_{VV}^0 : Sigma nought calibrated Sentinel-1 Vertical-Vertical (VV) polarization

$\sigma_{VV(max)}^0$: Maximum value of sigma nought calibrated Sentinel-1 Vertical-Vertical (VV) polarization

Just like the Normalized Difference Vegetation Index (NDVI) [34], DPSVI is proportional to vegetation biophysical information. For example, the higher the DPSVI value, the higher the vegetation biomass will be. Referring to Ref. 30 research, DPSVI is accurate enough to extract vegetation biophysical information from dual-polarized C-band SAR imageries such as Sentinel-1. Therefore, in this research, DPSVI is used as a parameter to test the ability of each speckle filtering method on Sentinel-1 imagery to extract vegetation biophysical information.

3.4 Accuracy Assessment and Sampling

The accuracy assessment is carried out using the Pearson Correlation Coefficient (PCC) (r), which is formulated as follows⁴¹:

$$r = \frac{\sum_{i=1}^n (x_i - \bar{x})(y_i - \bar{y})}{\sqrt{\sum_{i=1}^n (x_i - \bar{x})^2} \sqrt{\sum_{i=1}^n (y_i - \bar{y})^2}} \quad (2)$$

Where:

x_i : the i^{th} pixel of Sentinel-1 DPSVI

y_i : the i^{th} pixel of Sentinel-2 vegetation biophysical information

n : number of sample pixels

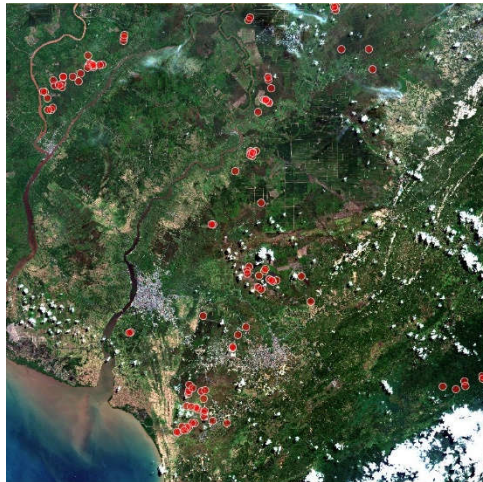


Fig. 6. Distribution of sample locations on Sentinel-2 MSI true color composite imagery.

In the calculation of PCC (r), a sample of a number of pixels is required. The distribution and designation of sample pixels is carried out with the help of the NDVI transformation of Sentinel-2 imagery. This is because NDVI has been shown to have a fairly strong correlation with vegetation biophysical information. The distribution of sample pixels was carried out by stratified purposive sampling. First, the vegetation features are separated from the non-vegetative features in NDVI. The technique is to use Otsu Thresholding²⁹. In this research, the Otsu Thresholding process was carried out using the free software Fiji is just ImageJ (Fiji)^{36,37}. From the results of Otsu Thresholding, a threshold value of 0.3 is obtained, this means that the NDVI value of 0.3 to 1 is confirmed to be vegetation features. The NDVI values of 0.3 to 1 are then stratified into ten strata. Next, the sample pixels are distributed purposively in each stratum. The distribution of these sample pixels is sufficient to represent almost all types of land cover in the study area, such as dryland forest, swamp forest, peatland forest, mangrove forest, plantation forest, rubber plantation, oil palm plantation, mixed garden, fields/moorlands, rice fields, shrubs and bushes, swamp shrubs and bushes, and grasslands. In sampling, there are several areas to avoid, i.e. areas covered by clouds or cloud shadows on Sentinel-2 imagery, and areas experiencing geometric distortion on Sentinel-1 imagery, i.e. shadow, foreshortening, or layover.

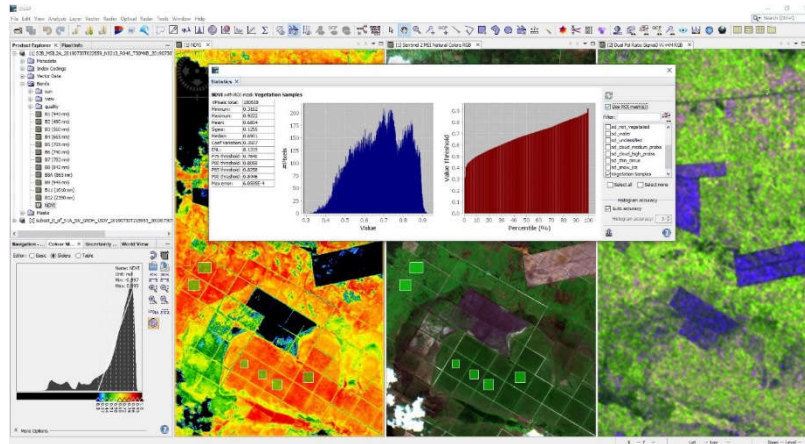


Fig. 7. Determination of sample pixels was done by stratified purposive sampling.

There are a total of more than 100,000 pixels set as samples. In the designation of sample pixels, the statistical distribution of NDVI values is of great concern. In this case, the distribution of pixel values of the NDVI sample is attempted to approach the normal distribution, although it cannot be completely normal, as shown in Fig. 6. Using the sample pixels, the PCC is then calculated in pairs between the DPSVI results from a certain speckle filtering method, and one of the variables from the vegetation biophysical information from Sentinel-2. For example, PCC between DPSVI filtered by Lee's method with a processing window size of 3x3 with LAI. And so on for other speckle filtering methods and other vegetation biophysical information variables.

3.5 Window Size Simulation

The target to be achieved in the search for the most optimal speckle filtering methods is to find a PCC value that reaches 0.8. Or in other words, the results of speckle filtering with vegetation biophysical information have a very strong correlation. If there is no PCC value that reaches 0.8 up to a processing window size of 21x21, then a simulation will be carried out to find the most optimal processing window size, so that later a PCC value of 0.8 can be obtained. The simulation of the processing window size was carried out using the regression method, based on the data of known PCC values up to the processing window size of 21x21. In this case, a scoring method is used on the processing window sizes. Namely, size 3x3 will be given a score of 3, size 5x5 will be given a score of 5, and so on, until size 21x21 will be given a score of 21. In the construction process of processing window size regression models, PCC values will be assigned as independent variables (x-axis). Meanwhile the processing window sizes will be placed as the dependent variable (y axis). The regression models applied are linear, exponential, logarithmic, power, and polynomial (quadratic). The regression equation which later has the highest correlation coefficient (r^2) is considered the best model to predict the most optimal processing window size in speckle filtering.

4. RESULT AND DISCUSSIONS

The many speckle filtering methods that are already available sometimes cause confusion when extracting certain information from SAR images such as Sentinel-1. This is the main thing that underlies this research. Indeed, up to now, there have been many studies comparing various speckle filtering methods. Either speckle filtering for things that are general, or specific for extracting vegetation information as is done in this research. From the point of view of SAR imagery, vegetation has its own characteristics based on its backscattering of electromagnetic waves burst by the SAR sensor. SAR technology is able to capture or distinguish between surface or specular features such as water and bare lands, double bounce features such as tall buildings or towers, and volumetric features such as vegetation canopy²⁷.

In this case, vegetation can have only volume scattering characteristics or a combination of volume scattering and double reflection scattering. If the vegetation has standing stems like trees, it will have a double bounce and scattering volume simultaneously. However, if the vegetation has only the structure of leaves and twigs without a stem, like a bush, then it will only have a scattering volume. Since speckle originating from the coherent summation of many individual feature scattering events within a pixel²⁷, vegetation features are among those that are quite problematic with speckle effects. This is caused by the structure of branches, twigs, and leaves of vegetation which will scatter electromagnetic waves from the SAR sensor in various directions irregularly.

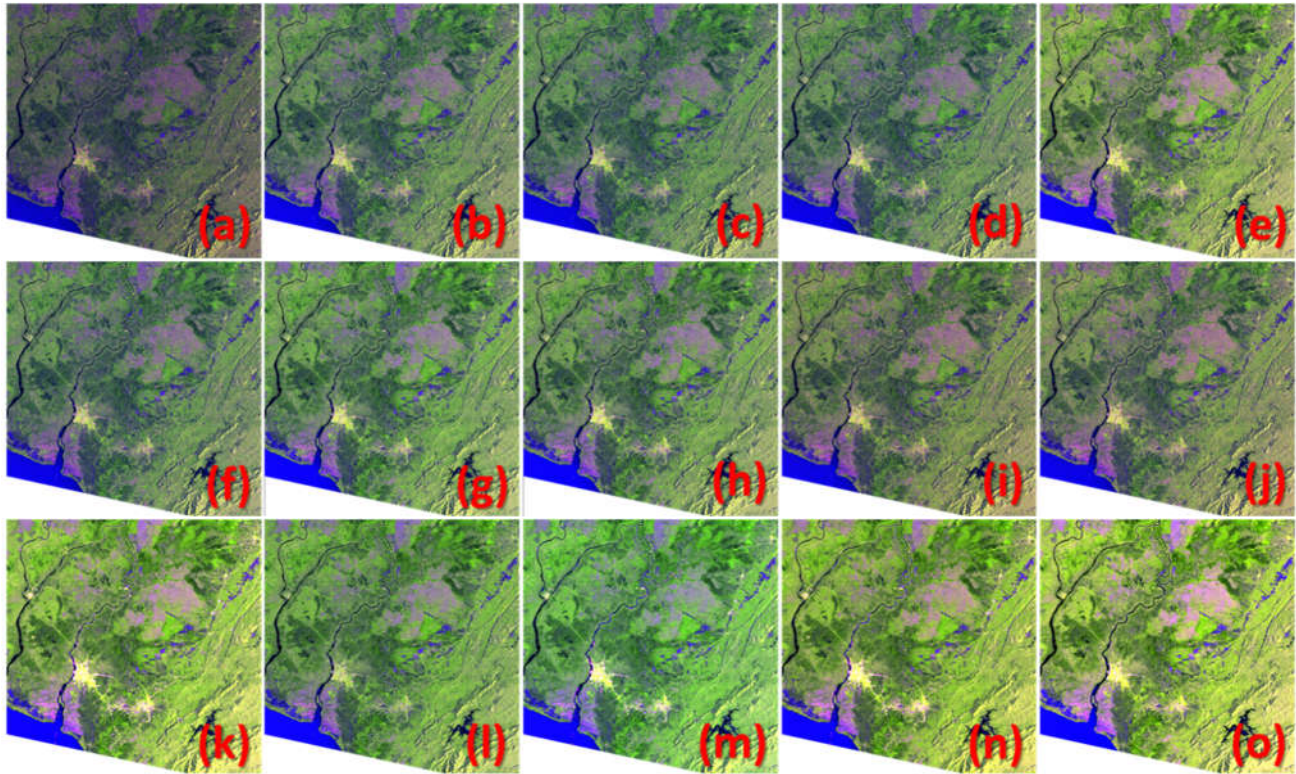


Fig. 8. Unfiltered Sentinel-1 imagery and speckle filtered Sentinel-1 imageries. (a) Original imagery (unfiltered); (b) Boxcar 3x3; (c) Frost 3x3; (d) Gamma Map 3x3; (e) IDAN; (f) Lee 3x3; (g) Lee Sigma 7x7 (target window 3x3); (h) Lee Sigma 7x7 (target window 5x5); (i) Median 3x3; (j) Refined Lee; (k) Boxcar 37x37; (l) Frost 49x49; (m) Gamma Map 37x37; (n) Lee 37x37; and (o) Median 37x37.

One of the main problems faced in speckle filtering is the execution process which is very time consuming. In this research we have used a workstation computer with a Core-i7 processor, 32 GB memory, and a fast PCIe Solid State Drive (SSD) hard drive. However, the process still feels quite heavy. The larger the processing window size, the heavier the process will be. Thus, large processing window sizes in speckle filtering may be very impractical for certain purposes. Furthermore, for the purposes of processing one full swath of Sentinel-1 imagery or larger, we do not recommend applying a processing window size that is large enough for computer specifications with less than 8 GB of memory and non-SSD hard drives.

In total, there were 71 times of speckle filtering processing applied in this study. Therefore, this will produce an output of 71 speckle filtered imageries. Of course, it is not possible to visually present all the filtering results in this paper. In Fig. 8, we only present speckle filtered image samples with the default settings from the SNAP application, plus 5 speckle filtered simulation results. More details about the number of the outputs can be seen in Table 1 and Table 2. Usually, speckle filtering performances were assessed using Root Mean Square Error (RMSE), Peak Signal to Noise Ratio (PSNR), Mean Structural Similarity Index Measure (MSSIM), Edge Preservation Index (EPI), or Equivalent Number of Looks (ENL). However, the accuracy assessment in this research is carried out using the Pearson Correlation Coefficient (PCC) or r values, which were calculated in pairs between DPSVI from speckle filtering results and vegetation biophysical information. This is because our target is to find the most accurate speckle filtering in the context of extracting vegetation biophysical information. Without paying too much attention to the presence of other features around the vegetation object.

Based on the results of the r calculation, it is clearly seen in Table 1 that for speckle filtering methods with the default parameter settings of the SNAP application, IDAN is able to provide the best results. Followed by Lee Sigma, Boxcar, Lee, Gamma Map, Refined Lee, Frost, and Median respectively. Therefore, for practical purposes in terms of extracting vegetation biophysical information, we could recommend IDAN or Lee Sigma. Indeed, speckle filtering using IDAN with its own default parameters is actually quite time consuming, compared to other methods. IDAN's best ability in this research is in line with the results of previous research²⁶. IDAN filter is able to reduce noise speckle significantly, but at the same time preserve fine detail and prevent blurring effect²⁶.

Table 1. PCC (r) values between DPSVI and vegetation biophysical information in each speckle filtering method.

| Speckle Filters | Parameters | Parameter Scoring | LAI | CWC | CCC | FVC | FAPAR |
|-------------------------------------|------------|-------------------|----------|----------|----------|----------|----------|
| Unfiltered | - | - | 0.296052 | 0.308913 | 0.263586 | 0.303591 | 0.311245 |
| Refined Lee | Default | - | 0.402843 | 0.419640 | 0.359107 | 0.413021 | 0.423679 |
| IDAN | Default | - | 0.560491 | 0.583778 | 0.500419 | 0.574348 | 0.589653 |
| Boxcar | 3x3* | 3 | 0.406172 | 0.422591 | 0.362794 | 0.416114 | 0.426334 |
| | 5x5 | 5 | 0.500568 | 0.520607 | 0.447841 | 0.512511 | 0.525250 |
| | 7x7 | 7 | 0.558434 | 0.580951 | 0.500135 | 0.571207 | 0.585663 |
| | 9x9 | 9 | 0.594633 | 0.619022 | 0.533044 | 0.607551 | 0.623243 |
| | 11x11 | 11 | 0.619269 | 0.645131 | 0.555676 | 0.631900 | 0.648513 |
| | 13x13 | 13 | 0.637250 | 0.664230 | 0.572488 | 0.649237 | 0.666527 |
| | 15x15 | 15 | 0.651037 | 0.678911 | 0.585718 | 0.662157 | 0.679973 |
| | 17x17 | 17 | 0.661868 | 0.690583 | 0.596318 | 0.672075 | 0.690300 |
| | 19x19 | 19 | 0.670407 | 0.699904 | 0.604730 | 0.679843 | 0.698342 |
| | 21x21 | 21 | 0.677627 | 0.707795 | 0.611872 | 0.686452 | 0.705157 |
| Frost | 3x3* | 3 | 0.403614 | 0.419940 | 0.360471 | 0.413520 | 0.423675 |
| | 5x5 | 5 | 0.489715 | 0.509239 | 0.438050 | 0.501473 | 0.513861 |
| | 7x7 | 7 | 0.541677 | 0.563361 | 0.485058 | 0.554118 | 0.567965 |
| | 9x9 | 9 | 0.574386 | 0.597673 | 0.514799 | 0.586902 | 0.601795 |
| | 11x11 | 11 | 0.596065 | 0.620611 | 0.534476 | 0.608524 | 0.624166 |
| | 13x13 | 13 | 0.610811 | 0.636241 | 0.547831 | 0.623213 | 0.639334 |
| | 15x15 | 15 | 0.620996 | 0.647026 | 0.557179 | 0.633248 | 0.649707 |
| | 17x17 | 17 | 0.628129 | 0.654575 | 0.563837 | 0.640159 | 0.656878 |
| | 19x19 | 19 | 0.633118 | 0.659860 | 0.568570 | 0.644933 | 0.661835 |
| | 21x21 | 21 | 0.636597 | 0.663570 | 0.571904 | 0.648247 | 0.665272 |
| Gamma Map | 3x3* | 3 | 0.405113 | 0.421601 | 0.361773 | 0.415049 | 0.425135 |
| | 5x5 | 5 | 0.496994 | 0.517203 | 0.444361 | 0.508978 | 0.521408 |
| | 7x7 | 7 | 0.550687 | 0.572854 | 0.492963 | 0.563386 | 0.577288 |
| | 9x9 | 9 | 0.586070 | 0.610063 | 0.525235 | 0.598720 | 0.613935 |
| | 11x11 | 11 | 0.613891 | 0.640094 | 0.550319 | 0.626397 | 0.642810 |
| | 13x13 | 13 | 0.634122 | 0.661834 | 0.568934 | 0.646281 | 0.663470 |
| | 15x15 | 15 | 0.648051 | 0.676678 | 0.582215 | 0.659451 | 0.677165 |
| | 17x17 | 17 | 0.658896 | 0.688350 | 0.592848 | 0.669302 | 0.687467 |
| | 19x19 | 19 | 0.667553 | 0.697679 | 0.601475 | 0.677001 | 0.695482 |
| | 21x21 | 21 | 0.674986 | 0.705630 | 0.609010 | 0.683636 | 0.702355 |
| Lee | 3x3* | 3 | 0.405462 | 0.421876 | 0.362130 | 0.415402 | 0.425554 |
| | 5x5 | 5 | 0.497538 | 0.517368 | 0.445103 | 0.509424 | 0.521971 |
| | 7x7 | 7 | 0.553706 | 0.575792 | 0.495919 | 0.566337 | 0.580530 |
| | 9x9 | 9 | 0.590880 | 0.614774 | 0.529834 | 0.603528 | 0.619005 |
| | 11x11 | 11 | 0.616842 | 0.642215 | 0.553616 | 0.629220 | 0.645608 |
| | 13x13 | 13 | 0.635423 | 0.662066 | 0.570844 | 0.647303 | 0.664352 |
| | 15x15 | 15 | 0.649455 | 0.677149 | 0.584167 | 0.660640 | 0.678217 |
| | 17x17 | 17 | 0.660473 | 0.689117 | 0.594870 | 0.670770 | 0.688803 |
| | 19x19 | 19 | 0.669288 | 0.698704 | 0.603586 | 0.678705 | 0.697074 |
| | 21x21 | 21 | 0.676754 | 0.706738 | 0.611098 | 0.685412 | 0.704030 |
| Median | 3x3* | 3 | 0.385276 | 0.401832 | 0.343492 | 0.394951 | 0.404840 |
| | 5x5 | 5 | 0.478489 | 0.499476 | 0.426043 | 0.491120 | 0.504198 |
| | 7x7 | 7 | 0.539055 | 0.562399 | 0.480472 | 0.552485 | 0.567756 |
| | 9x9 | 9 | 0.578467 | 0.603073 | 0.515982 | 0.592425 | 0.609261 |
| | 11x11 | 11 | 0.604744 | 0.630421 | 0.539959 | 0.618587 | 0.636504 |
| | 13x13 | 13 | 0.623689 | 0.650491 | 0.557393 | 0.637082 | 0.655747 |
| | 15x15 | 15 | 0.637261 | 0.664975 | 0.570080 | 0.650090 | 0.669203 |
| | 17x17 | 17 | 0.648717 | 0.676957 | 0.581104 | 0.660778 | 0.680255 |
| | 19x19 | 19 | 0.657876 | 0.686680 | 0.589989 | 0.669118 | 0.688895 |
| | 21x21 | 21 | 0.666001 | 0.695224 | 0.597863 | 0.676586 | 0.696588 |
| Lee Sigma (Target Window Size 3x3*) | 5x5 | 5 | 0.458273 | 0.478633 | 0.410470 | 0.467116 | 0.477632 |
| | 7x7* | 7 | 0.492558 | 0.515541 | 0.441533 | 0.501112 | 0.512294 |
| | 9x9 | 9 | 0.511214 | 0.535856 | 0.458516 | 0.519460 | 0.531077 |
| | 11x11 | 11 | 0.522779 | 0.548637 | 0.469182 | 0.530513 | 0.542501 |
| | 13x13 | 13 | 0.530884 | 0.557580 | 0.476849 | 0.537972 | 0.550220 |
| | 15x15 | 15 | 0.537240 | 0.564687 | 0.483119 | 0.543532 | 0.556024 |
| Lee Sigma (Target Window Size 5x5) | 17x17 | 17 | 0.542143 | 0.570082 | 0.488110 | 0.548082 | 0.560726 |
| | 5x5 | 5 | 0.447942 | 0.468408 | 0.401217 | 0.455599 | 0.465458 |
| | 7x7* | 7 | 0.479107 | 0.502305 | 0.429655 | 0.485929 | 0.496351 |
| | 9x9 | 9 | 0.495054 | 0.520080 | 0.444272 | 0.501220 | 0.512074 |
| | 11x11 | 11 | 0.505303 | 0.531432 | 0.453770 | 0.510875 | 0.521946 |
| | 13x13 | 13 | 0.512040 | 0.539001 | 0.460174 | 0.516981 | 0.528226 |
| | 15x15 | 15 | 0.516941 | 0.544539 | 0.465053 | 0.521155 | 0.532538 |
| 17x17 | 17 | 0.520409 | 0.548459 | 0.468659 | 0.524069 | 0.535504 | |

* SNAP default window processing sizes

Henceforward, the results of testing the processing window size up to 21x21 show that Boxcar with a processing window size of 21x21 is the best speckle filtering method, as shown in Table 1. The ability of Boxcar with a 21x21 window applies to all vegetation biophysical information parameters tested in this study, namely LAI, CWC, CCC, FVC, and FAPAR. Boxcar's abilities are followed by Lee, Gamma Map, Median, and Frost respectively. Each with a processing window size of 21x21, and overall with r values of 0.6s to 0.7s.

Most comparative research of speckle filtering methods generally only presents speckle filtering trials at default settings, for example Lee with a processing window size of 3x3, or setting some variations of processing window sizes. This is what distinguishes this research from previous research. Because in this research, if no values of r were found that reach 0.8, then simulations will be implemented to determine the most optimal processing window sizes for the extraction of certain biophysical vegetations. Of course, not all speckle filtering methods tested in this research can be included in the simulation, because some speckle filtering methods set a fixed processing window size or limit the processing window to a certain size. In fact, from the test results of all speckle filtering methods up to a processing window size of 21x21, no r value of 0.8 was found. Therefore, the decision is to do a simulation or modeling using the regression method, to estimate what the most optimal window size is so that an r value of 0.8 can be achieved for each speckle filtering method, on each vegetation biophysical information parameter.

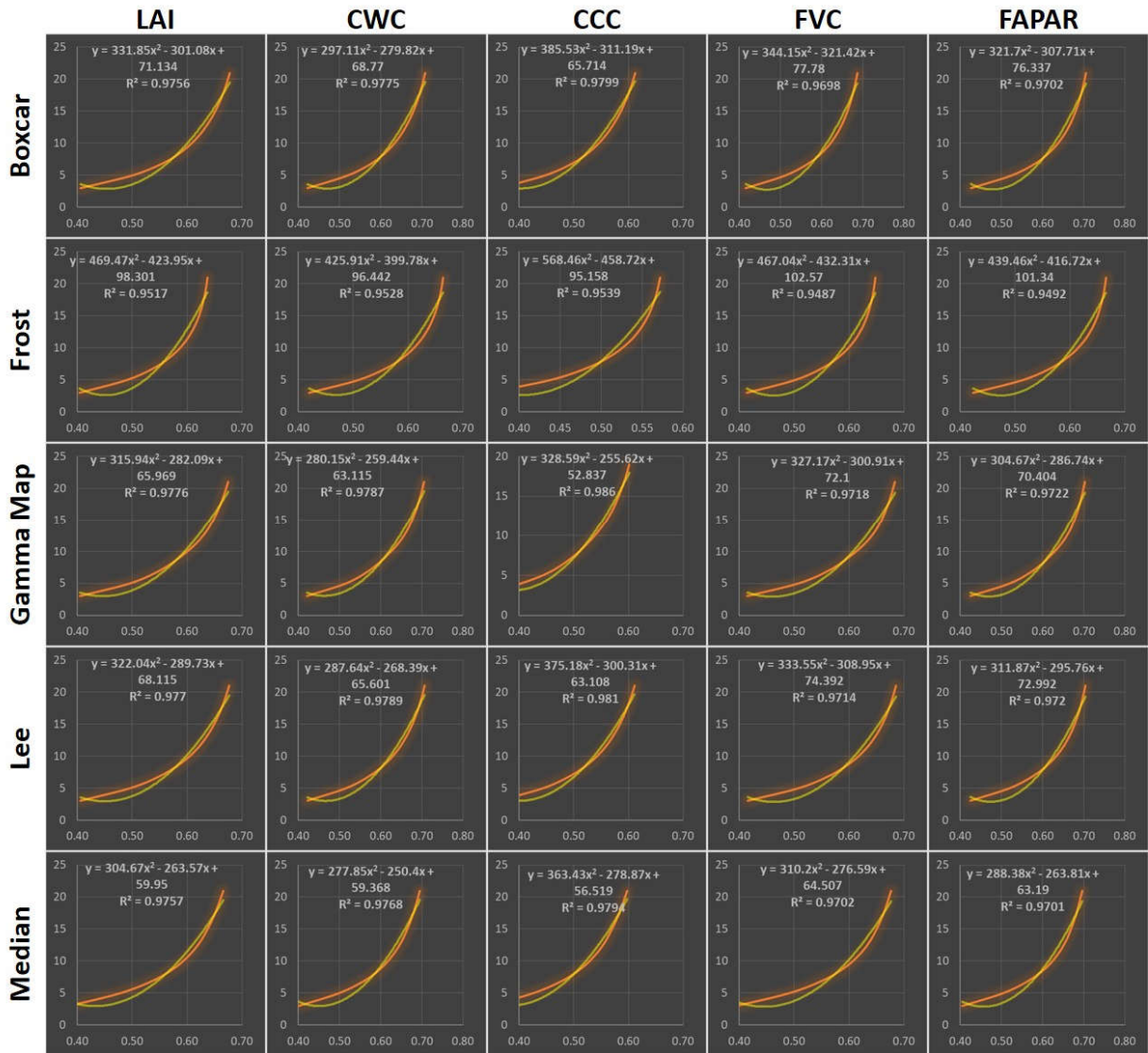


Fig. 9. Regression models to predict the most optimal processing window sizes.

Fig. 9 shows the simulation results of processing window sizes to reach r values up to 0.8. The entire speckle filtering method for each vegetation biophysical information parameter shows a polynomial (quadratic) correlation with increasing processing window sizes. In Fig. 9, we only present the test regression models with the highest correlation coefficients (r^2). Because it would be too much if we had to display graphs for all the regression models tested in this study. Overall r^2 shows a value of 0.9 more, this means between the increase in processing window sizes with accuracy (r). However, since the correlations are quadratic, it could be predicted that at some point the values of r will be saturated, even though the processing window sizes in speckle filtering are enlarged. In other words, increasing the processing window sizes to certain sizes will no longer be able to significantly increase the accuracy of the speckle filtering methods.

In order to assess the simulation results of processing window sizes, we sampled one of the vegetation biophysical information parameters, namely FAPAR, to be tested on five speckle filtering methods, namely Boxcar, Frost, Gamma Map, Lee, Median. Each with the window size of the simulation results as shown in Table 1, in the FAPAR column. Boxcar, Gamma Map, Lee, and Median, were tested using a size of 37x37, while Frost was tested using a size of 49x49. These 37x37 and 49x49 measures were calculated using the quadratic regression models in Fig. 9, specifically for FAPAR. If the quadratic regression calculation processes produce a number that is not odd, then the result of the calculation process will be rounded up to the odd number above it. For example, one calculation process results in the number 36 or 36.24, it will be rounded to 37. This is because the processing window sizes in speckle filtering or image filtering in general must be odd numbers, such as 37x37. Of course, the size of 37x37 let alone 49x49 is the size of the speckle filtering window which is quite large, so it will require quite high computer resources. Furthermore, it appears that overall, to reach an r value of 0.8, processing window sizes ranging from 35x35 to 93x93 are required for certain vegetation biophysical information parameters.

Table 2. Estimated processing window sizes for each method of speckle filtering and vegetation biophysical information to reach a PCC value of 0.8.

| | LAI | CWC | CCC | FVC | FAPAR |
|-----------|---------|---------|---------|---------|---------|
| Boxcar | 43 x 43 | 35 x 35 | 65 x 65 | 41 x 41 | 37 x 37 |
| Frost | 61 x 61 | 49 x 49 | 93 x 93 | 57 x 57 | 49 x 49 |
| Gamma Map | 43 x 43 | 35 x 35 | 59 x 59 | 41 x 41 | 37 x 37 |
| Lee | 43 x 43 | 35 x 35 | 63 x 63 | 41 x 41 | 37 x 37 |
| Median | 45 x 45 | 37 x 37 | 67 x 67 | 43 x 43 | 37 x 37 |

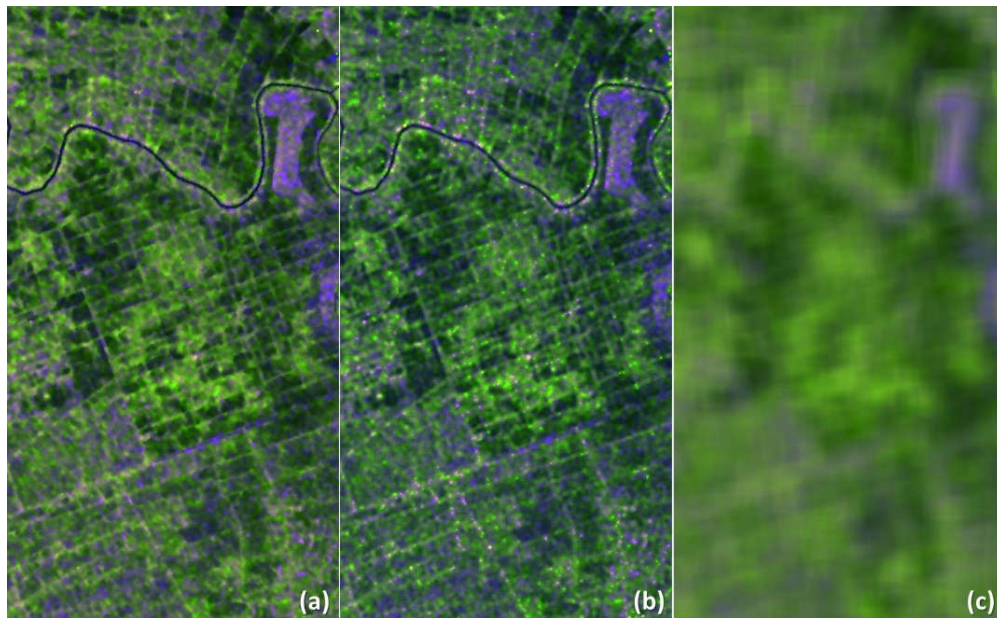


Fig. 10. Visual comparison between (a) IDAN, (b) Lee Sigma 7x7 (target window size 3x3), and (c) Boxcar 37x37.

The results of the speckle filtering using the simulated window sizes were then retested using PCC. The test results show that the r value for Boxcar is 0.735194, the r value for Frost is 0.668937, the r value for Gamma Map is 0.730305, the r value for Lee is 0.733073, and the r value for Median is 0.730752. Even though the r values increase after the processing window sizes are enlarged by simulation, however the results of this assessment are below expectations, where the resulting r values expected to be around 0.8. Our prediction is that this is due to the insufficient sample size of the speckle filtering window in the construction of the regression models. As a result, the regression models produced in this research are overestimated. In the construction of regression models there are only 10 samples, namely from window sizes 3x3 to 21x21. In fact, to build an objective regression model, at least 30 data samples are needed. It may be necessary to further study at least to prepare a sufficient number of samples of speckle filtering window sizes.

In addition to requiring adequate computer hardware, there are other implications that will be experienced by SAR images when the processing window size is large enough. Among them are the decrease in the spatial resolution of the image and the blur effect on the image, as shown in Fig. 10. So that although on the one hand it is advantageous, namely by increasing the correlation value or accuracy, but this can also be detrimental. Because we will lose certain details in the image. Thus, the use of a sufficiently large processing window in speckle filtering must also be carefully considered. The capabilities of IDAN and Lee Sigma are almost equal, if each with default settings. Both are able to reduce speckle effects significantly, while maintaining detail on the image well. However, there is one drawback to Lee Sigma. Namely having the presence of bright spots on certain features, as shown in Fig. 10. Where this is not experienced by the IDAN filter. So that in this case IDAN is indeed superior compared with Lee Sigma, both statistically and visually. The similarity between IDAN and Lee Sigma is that for IDAN the processing window size is fixed, so it cannot be changed, and for Lee Sigma, the processing window size setting is very limited.

5. CONCLUSIONS

In this research, we focus more on presenting a comparison of the capabilities of several speckle filtering methods to extract various vegetation biophysical information parameters. Without having to review further the fundamental concepts of each speckle filtering method. The results of the research show that in setting the default parameters using SNAP software, IDAN and Lee Sigma are able to provide the best performance. However, these two filters are less flexible in setting processing window sizes. When the processing window sizes are set to 21x21, the Boxcar method and Lee's method give the best results, with the PCC values ranging from 0.6s to 0.7s. Even when processing window sizes are simulated to reach a PCC value of 0.8, Boxcar still delivers the best output. Despite the fact that the PCC value of 0.8 was never achieved in this research, this was due to the limited number of samples in the simulation. Of course, with the consequence of decreasing the spatial resolution of the image and losing certain details on the image.

ACKNOWLEDGEMENTS

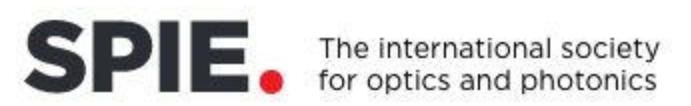
This research was funded by the Center for Geospatial Information Infrastructure Development (PPIIG) of Universitas Lambung Mangkurat, Banjarbaru, Indonesia. We thank the European Space Agency (ESA) which has provided Sentinel-1 SAR imagery, Sentinel-2 MSI imagery, and SNAP software for free. And also to the Geospatial Information Laboratory, Faculty of Forestry, Universitas Lambung Mangkurat, which has facilitated digital imagery processing in this research.

REFERENCES

- [1] Arienzo, A., Argenti, F., Alparone, L. and Gherardelli, M., "Accurate Despeckling and Estimation of Polarimetric Features by Means of a Spatial Decorrelation of the Noise in Complex PolSAR Data," *Remote Sensing* 12 (2), 331 (2020).
- [2] Attema E. P. W. and Ulaby, F. T., "Vegetation modeled as a water cloud," *Radio Science* 13 (2), 357-364 (1978).
- [3] Baghdadi, N., El Hajj, M., Zribi, M. and Bousbih, S., "Calibration of the Water Cloud Model at C-Band for Winter Crop Fields and Grasslands," *Remote Sensing* 9 (9), 969 (2017).
- [4] Bai, X., He, B., Li, X., Zeng, J., Wang, X., Wang, Z., Zeng, Y. and Su, Z., "First Assessment of Sentinel-1A Data for Surface Soil Moisture Estimations Using a Coupled Water Cloud Model and Advanced Integral Equation Model over the Tibetan Plateau," *Remote Sensing* 9 (7), 714 (2017).

- [5] Bao, Y., Lin, L., Wu, S., Kwal Deng, K. A. and Petropoulos, G. P., "Surface soil moisture retrievals over partially vegetated areas from the synergy of Sentinel-1 and Landsat 8 data using a modified water-cloud model," *International Journal of Applied Earth Observation and Geoinformation* 72, 76-85 (2018).
- [6] Baraldi, A. and Parmigiani, F., "A Refined Gamma MAP SAR Speckle Filter with Improved Geometrical Adaptivity," *IEEE Transactions on Geoscience and Remote Sensing* 33 (5), 1245-1257 (1995).
- [7] Bouchemakh, L., Smara, Y., Boutarfa, S. and Hamadache, Z., "A Comparative Study of Speckle Filtering In Polarimetric Radar SAR Images," 2008 3rd International Conference on Information and Communication Technologies: From Theory to Applications, 1-6 (2008).
- [8] Brown, L. A., Fernandes, R., Djamai, N., Meier, C., Gobron, N., Morris, H., Canisius, F., Bai, G., Lerebourg, C., Lanconelli, C., Clerici, M. and Dash, J., "Validation of baseline and modified Sentinel-2 Level 2 Prototype Processor leaf area index retrievals over the United States," *ISPRS Journal of Photogrammetry and Remote Sensing* 175, 71-87 (2021).
- [9] Djamai, N., Fernandes, R., Weiss, M., McNairn, H. and Goïta, K., "Validation of the Sentinel Simplified Level 2 Product Prototype Processor (SL2P) for mapping cropland biophysical variables using Sentinel-2/MSI and Landsat-8/OLI data," *Remote Sensing of Environment* 225, 416-430 (2019).
- [10] Farage, G., Foucher, S. and Benie, G., "Comparison of PolSAR Speckle Filtering Techniques," 2006 IEEE International Symposium on Geoscience and Remote Sensing, 1760-1763 (2006).
- [11] Foucher, S. and López-Martínez, C., "Analysis, Evaluation, and Comparison of Polarimetric SAR Speckle Filtering Techniques," *IEEE Transactions on Image Processing* 23, 1751-1764 (2014).
- [12] Frost, V.S., Stiles, J. A., Shanmugan, K. S. and Holtzman, J., "A Model for Radar Images and Its Application to Adaptive Digital Filtering of Multiplicative Noise," *IEEE Transactions on Pattern Analysis and Machine Intelligence* 4 (2), 157-165 (1982).
- [13] Garioud, A., Valero, S., Giordano, S. and Mallet, C., "Recurrent-based regression of Sentinel time series for continuous vegetation monitoring," *Remote Sensing of Environment* 263, 112419 (2021).
- [14] Giri Ananto, W. H., Putri, A. F. S., Hadi, H. A., Hanum, D. N., Wiryawan, W. K. P., Prabaswara, R. R. and Arjasakusuma, S., "Performance of various speckle filter methods in modelling forest aboveground biomass using Sentinel-1 data: case study of Barru Regency, South Sulawesi," *Proceedings of SPIE* 11311, Sixth Geoinformation Science Symposium, 113110P (21 November 2019).
- [15] Graham, A. J. and Harris, R., "Extracting biophysical parameters from remotely sensed radar data: a review of the water cloud model," *Progress in Physical Geography: Earth and Environment* 27 (2), 217-229 (2003).
- [16] Kang, Y., Ozdogan, M., Gao, F., Anderson, M. C., White, W. A., Yang, Y., Yang, Y. and Erickson, T. A., "A data-driven approach to estimate leaf area index for Landsat images over the contiguous US," *Remote Sensing of Environment* 258, 112383 (2021).
- [17] Kganyago, M., Mhangara, P., Alexandridis, T., Laneve, G., Ovakoglou, G. and Mashiyi, N., "Validation of sentinel-2 leaf area index (LAI) product derived from SNAP toolbox and its comparison with global LAI products in an African semi-arid agricultural landscape," *Remote Sensing Letters* 11 (10), 883-892 (2020).
- [18] Lang, S., Lin, C. Y., Liu, J., Wong, N., Kwok-Hay So, H., "A comparison of SAR image speckle filters," *Proceedings of SPIE* 7498, MIPPR 2009: Remote Sensing and GIS Data Processing and Other Applications, 749804 (30 October 2009).
- [19] Lee, J. S., "Speckle analysis and smoothing of synthetic aperture radar images," *Computer Graphics and Image Processing* 17 (1), 1981, 24-32 (1981).
- [20] Lee, J. S., "A simple speckle smoothing algorithm for synthetic aperture radar images," *IEEE Transactions on System, Man, and Cybernetics SMC-13* (1), 85-89, (1983).
- [21] Lee, J. S., "Digital image smoothing and the sigma filter," *Computer Vision, Graphics, and, Image Processing* 24 (2), 255-269, (1983).
- [22] Lee, J. S., Jurkevich, J., Dewaele, P., Wambacq, P. and Oosterlinck, A., "Speckle filtering of synthetic aperture radar images: A review," *Remote Sensing Reviews* 8 (4), 313-340 (1994).
- [23] Lee, J. S., Grunes, M. R. and de Grandi, G., "Polarimetric SAR speckle filtering and its implication for classification," *IEEE Transactions on Geoscience and Remote Sensing* 37 (5), 2363-2373 (1999).
- [24] Mandal, D., Kumar, V., Ratha, D., Dey, S., Bhattacharya, A., Lopez-Sanchez, J. M., McNairn, H. and Rao, Y. S., "Dual polarimetric radar vegetation index for crop growth monitoring using sentinel-1 SAR data," *Remote Sensing of Environment* 247, 111954 (2020).

- [25] Mandal D., Kumar, V., Lopez-Sanchez, J. M., Bhattacharya, A., McNairn, H. and Rao, Y. S., "Crop biophysical parameter retrieval from Sentinel-1 SAR data with a multi-target inversion of Water Cloud Model," *International Journal of Remote Sensing* 41 (14), 5503-5524 (2020).
- [26] Medasani, S. and Reddy, G. U., "Analysis and Evaluation of Speckle Filters for Polarimetric Synthetic Aperture Radar (PolSAR) Data," *International Journal of Applied Engineering Research* 12 (15), 4916-4927 (2017).
- [27] Meyer, F., "Spaceborne Synthetic Aperture Radar: Principles, Data Access, and Basic Processing Techniques," in Flores-Anderson, A. I., Herndon, K. E., Thapa, R. B., and Cherrington, E., (eds.), [The Synthetic Aperture Radar (SAR) Handbook: Comprehensive Methodologies for Forest Monitoring and Biomass Estimation], SERVIR Global Science, 21-63 (2019).
- [28] Morandeira, N. S., Grimson, R. and Kandung, P., "Assessment of SAR speckle filters in the context of object-based image analysis," *Remote Sensing Letters* 7 (2), 150-159 (2016).
- [29] Otsu, N., "A Threshold Selection Method from Gray-level Histograms," *IEEE Transactions on Systems, Man, and Cybernetics* 9, 62-69 (1979).
- [30] Periasamy, S., "Significance of dual polarimetric synthetic aperture radar in biomass retrieval: An attempt on Sentinel-1," *Remote Sensing of Environment* 217, 537-549 (2018).
- [31] Potapov, P., Tyukavina, A., Turubanova, S., Talero, Y., Hernandez-Serna, A., Hansen, M.C., Saah, D., Tenneson, K., Poortinga, A., Aekakkararungroj, A., Chishtie, F., Towashiraporn, P., Bhandari, B., Aung, K.S. and Nguyen, Q.H., "Annual continuous fields of woody vegetation structure in the Lower Mekong region from 2000-2017 Landsat time-series," *Remote Sensing of Environment* 232, 111278 (2019).
- [32] Ramesh, J. P., Badruddin, S.S. and Waghji, K. P., "Comparative Study of Gaussian and Box-Car Filter of TerraSAR-X Data Image using Pol-SAR for Speckle Noise Reduction," *International Journal of Recent Scientific Research* 9 (5), 26977-26980 (2018).
- [33] Richards, J. A., [Remote Sensing with Imaging Radar], Springer-Verlag, Berlin Heidelberg, 120 (2009).
- [34] Rouse, J. W., Haas, R. H., Schell, J. A. and Deering, D. W., "Monitoring vegetation systems in the Great Plains with ERTS," *Third ERTS Symposium NASA SP-351 I*, 309-317 (1973).
- [35] Santoso, A.W., Bayuaji, L., Sze, L. T., Lateh, H. and Zain, J. M., "Comparison of Various Speckle Noise Reduction Filters on Synthetic Aperture Radar Image," *International Journal of Applied Engineering Research* 11 (15), 8760-8767 (2016).
- [36] Schneider, C. A., Rasband, W. S. and Eliceiri, K. W., "NIH Image to ImageJ: 25 Years of Image Analysis," *Nature Methods* 9 (7), 671-675 (2012), PMID 22930834.
- [37] Schindelin, J., Rueden, C. T., Hiner, M. C. and Eliceiri, K. W., "The ImageJ Ecosystem: An open Platform for Biomedical Image Analysis," *Molecular Reproduction and Development*, (2015), PMID 26153368.
- [38] Sullivan, R., "Synthetic Aperture Radar," in Skolnik, M. I. (Editor in Chief), [Radar Handbook, Third Edition], The McGraw-Hill Companies, New York Chicago San Francisco Lisbon London Madrid Mexico City Milan New Delhi San Juan Seoul Singapore Sydney Toronto, 17.19-17.20 (2008).
- [39] Sun, S., Liu, R., Yang, C., Zhou, H., Zhao, J. and Ma, J., "Comparative study on the speckle filters for the very high-resolution polarimetric synthetic aperture radar imagery," *Journal of Applied Remote Sensing* 10 (4), 045014 (2016).
- [40] Vasile, G., Trouvé, E., Lee, J.S., and Buzuloiu, V., "Intensity-Driven Adaptive-Neighborhood Technique for Polarimetric and Interferometric SAR Parameters Estimation," *IEEE Transactions on Geoscience and Remote Sensing* 44 (6), 1609-1621 (2006).
- [41] Wang, J., "Pearson correlation coefficient," in Dubitzky W., Wolkenhauer O., Cho KH., Yokota H. (eds) [Encyclopedia of Systems Biology], Springer, New York, (2013).
- [42] Weiss, M. and Baret, F., S2ToolBox Level 2 products: LAI, FAPAR, FCOVER Version 1.1, (2016), https://step.esa.int/docs/extra/ATBD_S2ToolBox_L2B_V1.1.pdf.
- [43] Yadav, V. P., Prasad, R., Bala, R. and Srivastava, P. K., "Assessment of red-edge vegetation descriptors in a modified water cloud model for forward modelling using Sentinel-1A and Sentinel-2 satellite data," *International Journal of Remote Sensing* 42 (3), 794-804 (2021).
- [44] Yang, P., Verhoef, W., Prikaziuk, E. and van der Tol, C., "Improved retrieval of land surface biophysical variables from time series of Sentinel-3 OLCI TOA spectral observations by considering the temporal autocorrelation of surface and atmospheric properties," *Remote Sensing of Environment* 256, 112328 (2020).
- [45] Yommy, A. S., Liu, R. and Wu, A. S., "SAR Image Despeckling Using Refined Lee Filter," 2015 7th International Conference on Intelligent Human-Machine Systems and Cybernetics, 260-265 (2015).



Search

Manage Active Submissions

SPIE Submission System

Select Symposium:

Seventh Geoinformation Science Symposium (GSS 2021) (GSS21) ▾

Paper Title: **On finding optimal speckle filtering for extraction of vegetation biophysical information using Sentinel-1 SAR imagery**
Paper No. **GSS21-5**
Tracking No. **GSS21-GSS21-5**
Proceedings Coordinator: **Woods, Jenny** (JennyW@SPIE.org)

MANUSCRIPT

Status: Manuscript version 1 submitted and approved. Your copyright transfer form has been received.

Due Date

[Submit Manuscript Revision or Update Presentation Details](#)

25 September 2021

AUTHOR

▾ [Submission History](#)

Submission History

| revision title | date/time submitted | color pages | format conversion | author decision |
|--|----------------------|-------------|-------------------|-----------------|
| -1 On finding optimal speckle filtering for extraction of vegetation biophysical information using Sentinel-1 SAR imagery | 09 Sep 2021 00:03:14 | A4 | Yes | Approved |

* Indicates this version will be used for publication. To select a previous version, contact your staff proceedings coordinator.